MECHANICAL ENGINEERING SCIENCE

ISSN:2661-4448(online)
2661-443X(print)
Volume 6 No.1 2024

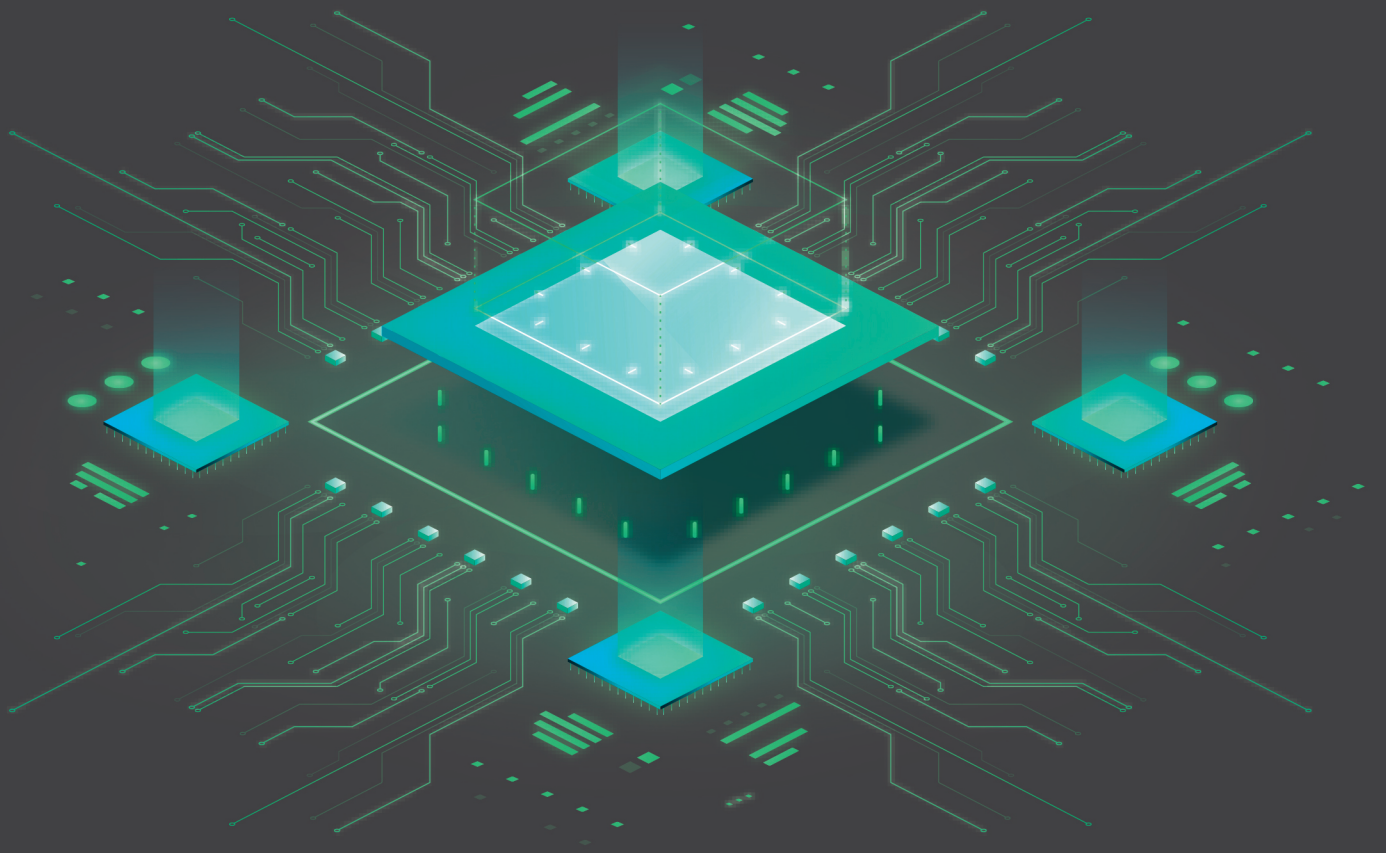

VISER
www.viserdata.com

COMPANY INTRODUCTION

Viser Technology Pte. Ltd. was founded in Singapore with branch offices in both Hebei and Chongqing, China. Viser focuses on publishing scientific and technological journals and books that promote the exchange of scientific and technological findings among the research community and around the globe. Despite being a young company, Viser is actively connecting with well-known universities, research institutes, and indexation database, and has already established a stable collaborative relationship with them. We also have a group of experienced editors and publishing experts who are dedicated to publishing high-quality journal and book contents. We offer the scholars various academic journals covering a variety of subjects and we are committed to reducing the hassles of scholarly publishing. To achieve this goal, we provide scholars with an all-in-one platform that offers solutions to every publishing process that a scholar needs to go through in order to show their latest finding to the world.

Mechanical Engineering Science

Publisher: Viser Technology Pte. Ltd.

ISSN: 2661-4448(online)
2661-443X(print)

Frequency: Semi-annual

Add.: 111 North Bridge Rd, #21-01 Peninsula Plaza, Singapore 179098

https://www.viserdata.com/

Mechanical Engineering Science

Volume 6 No.1 (2024)

CONTENTS

VISER

Viser Technology Pte. Ltd.
Mechanical Engineering Science
DOI: 10.33142/mes.v6i1.13221

Research Article Open Access

Computer Vision-Based Human Body Posture Correction System

Yangsen QIU, Yukun WANG, Yuchen WU, Xinyi QIANG, Yunzuo ZHANG *

School of Information science and Technology, Shijiazhuang Tiedao University, Shijiazhuang, Hebei, 050043, China

*Corresponding Author: Yunzuo ZHANG, E-mail: zhangyunzuo888@sina.com

Abstract

With the development of technology and the progress of life, more and more people, regardless of entertainment, learning, or work, cannot do without computer desks and cannot put down their mobile phones. Due to prolonged sitting and often neglecting the importance of posture, incorrect posture can often lead to health problems such as hunchback, lumbar muscle strain, and shoulder and neck pain over time. To address this issue, we designed a computer vision-based human body posture detection system. The system utilizes YOLOv8 technology to accurately locate key points of the human body skeleton, and then analyzes the coordinate positions and depth information of these key points to establish a criterion for distinguishing different postures. With the assistance of an SVM classifier, the system achieves an average recognition rate of 95%. Finally, we successfully deployed the posture detection system on Raspberry Pi hardware and conducted extensive testing. The test results demonstrate that the system can effectively detect various postures and provide real-time reminders to users to correct poor posture, demonstrating good practicality and stability.

Keywords: *computer vision; human posture; deep learning; image processing*

1 Introduction

With the development of modern society, the pressure of learning and work is increasing. People often need to sit for long periods to work and study, maintaining a correct sitting posture for an extended period is quite challenging, leading to various poor sitting postures such as hunching, leaning, and tilting. Prolonged incorrect sitting posture may lead to various health issues including hunchback, lumbar muscle strain, neck and shoulder pain, myopia, and strabismus, seriously affecting physical and mental health. Correct posture and posture are crucial for physical health. Therefore, we designed a computer vision-based human posture correction system aimed at timely reminding users of incorrect sitting postures through real-time posture recognition and voice broadcast technology, correcting erroneous sitting postures, and reducing the harm of poor sitting postures to the body. We hope to suppress health problems caused by incorrect posture from the root, help users improve poor posture, and prevent and reduce posture-related health problems. The system relies on deep learning training models, with high accuracy and real-time performance, while possessing good practicality and research significance, thereby helping users maintain the correct posture and ensure physical health.

2 System Architecture and Hardware Design

This system is mainly based on the Raspberry Pi 4B processor motherboard and Raspberry Pi Camera Module V2 camera. OpenCV is used as the platform for visual processing tasks, combined with YOLOv8 for object recognition and keypoint detection technology. The camera accurately locates the positions of the facial features and various skeletal points of the body, combined with SVM support vector machine model for posture judgment, and implements the function of correcting human sitting posture. If the posture is incorrect, an alarm and voice prompt will be issued. The system architecture is shown in Figure 1.

The system hardware mainly consists of the main processor Raspberry Pi 4B motherboard, camera module V2, LCD touchscreen, speaker module, power circuit, etc. The processor motherboard receives data from the LCD touchscreen to complete user-specified operations through parameter settings. Then, it processes the data from the camera module to judge and recognize the sitting posture, and the speaker module provides reminders. This system is compact and supports both Windows and Linux operating systems, suitable for small and portable designs overall. The circuit connection diagram is shown in Figure 2, and the physical

Received on May 15, 2024; Accepted on June 11, 2024

appearance of the system is shown in Figure 3.

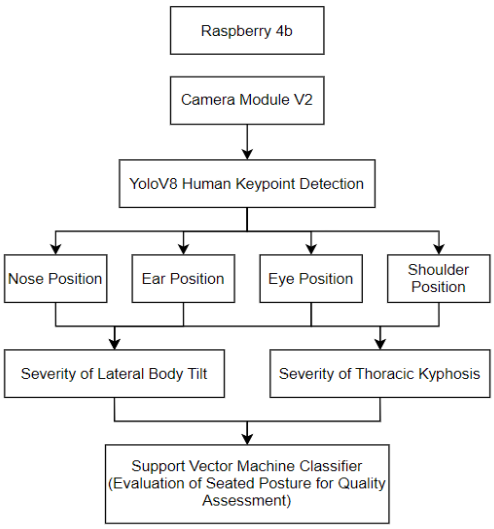

Figure 1 **System Architecture Diagram**

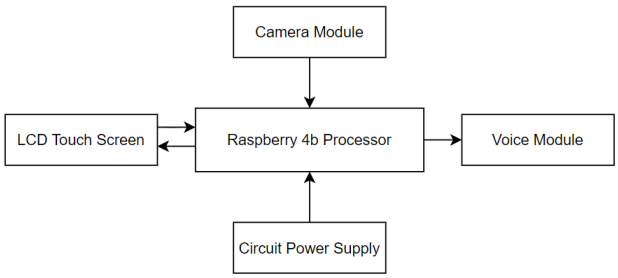

Figure 2 Circuit Connection Schematic Diagram

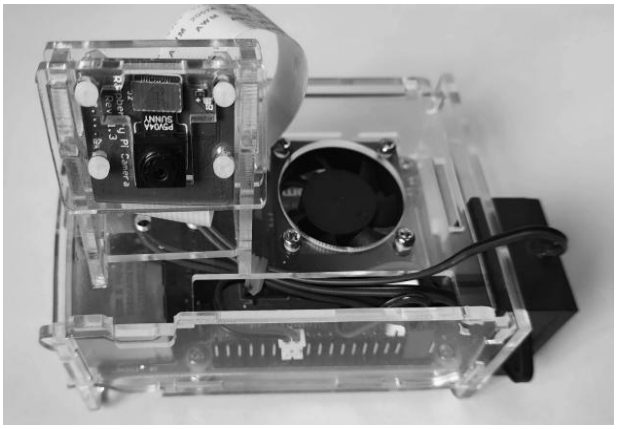

Figure 3 System Physical Appearance

3 Program and Algorithm Design

3.1 Program design

The main program flowchart is shown in Figure 4. After successful login and user operations, the model is first loaded. Simultaneously, the camera module is invoked, and upon collecting data, the captured video frames are passed to the system for processing. The system identifies the positions of key points such as eyes, nose, ears, and shoulders in the video frames. After processing with our designed algorithm, the human body posture in the video frame can be accurately distinguished. If the user adopts poor postures such as hunching or leaning, it will be marked as "bad" and a voice reminder will be issued; otherwise, it will be marked as "good". In addition to correcting poor postures, the system also sets reminders for prolonged sitting. If the user reaches the preset sitting time, the system will also issue a voice reminder.

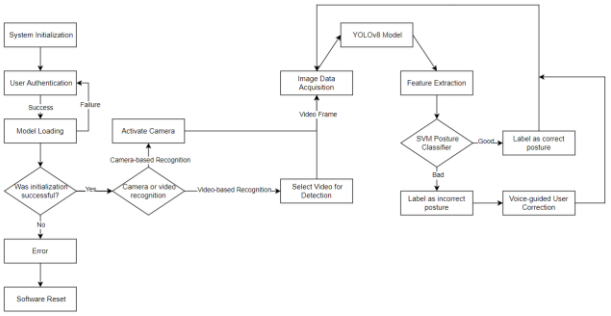

Figure 4 Main Program Flowchart

3.2 Algorithm design

3.2.1 Key-point detection and localization

In the human posture correction system, keypoint detection and localization are crucial stages based on computer vision technology. The neural network structure of this system is implemented based on the state-of-the-art object detection model - YOLOv8n, which integrates target detection and keypoint localization of the human body. The model network structure is divided into three parts: feature extraction network, feature fusion network, and detection head. Among them, the feature extraction network adopts CSPDarknet53, which includes a series of convolutional layers and residual blocks to extract high-level features from input images. The feature fusion network includes convolutional layers and upsampling layers to fuse feature maps of different resolutions, in order to better adapt to targets of different scales. Finally, the detection head consists of a series of convolutional layers and the final output layer, used to predict the positions of detection boxes and keypoint coordinates.

Figure 5 Key-point Connection Diagram

Additionally, we use two-dimensional arrays created with Numpy to store the keypoint coordinates output by the YOLOv8 model, including the positions of eyes, ears, nose, and shoulders. This provides reliable data support for subsequent posture analysis in the system, thereby achieving precise monitoring and analysis of user posture. The schematic diagram of keypoint connections is shown in Figure 5.

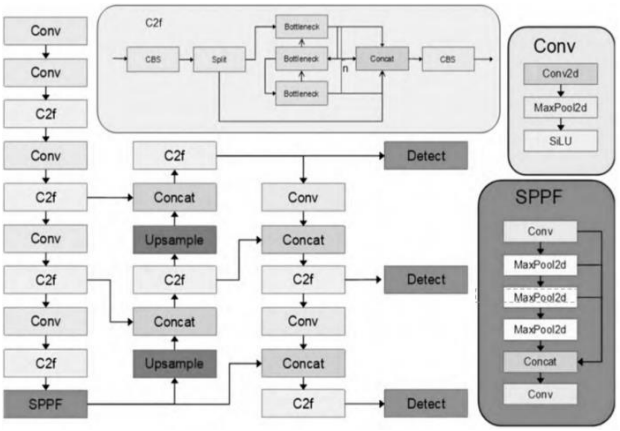

Figure 6 YOLOv8 Network Architecture

The YOLOv8 network architecture is depicted in Figure 6. It consists of an input end, Backbone, and Neck, describing the overall network structure. In YOLOv8, the input end adopts adaptive anchor calculation and adaptive grayscale padding. The backbone network includes Conv, C2f, and SPPF structures. The C2f module is mainly used to learn residual features and is inspired by the ELAN structure of YOLOv7. By introducing more branch cross-layer connections, it enhances the gradient flow of the model, forming a neural network module with stronger feature representation capability. Additionally, the Neck module adopts the PAN (path aggregation network) structure to enhance the network's ability to fuse features of objects at different scales.

3.2.2 Pose analysis and classification

In the stage of pose analysis and classification, this paper proposes to fuse the keypoint data mentioned above into two feature values, f1 and f2. These features are then inputted into an SVM classifier to accurately assess and classify the user's pose. The specific steps are as follows:

(1) Definition of Data to be Calculated

We first define the data to be calculated, including the coordinates of the left ear, right ear, left shoulder, and right shoulder, as well as the distances between these points. Specifically, the distance from the left ear to the left shoulder is defined as s1, the distance from the right ear to the right shoulder is defined as s2, and the distance from the left shoulder to the right shoulder is defined as s3. These are illustrated in Table 1 below.

To extract a representative midpoint for the positions of the left (right) eye, left (right) ear, and nose, and thus represent the center point of the body position, we choose to calculate the incenter coordinates of the triangle formed by these three points. The incenter is equidistant from the three sides of the triangle, making it a good representation of the central position of these three points. Using Equation 1 and Equation 2, we can obtain the coordinates of the left face midpoint, respectively. Similarly, we can derive the coordinates of the right face midpoint.

Table 1 Data Quantity Table

Data	Definition	Value
The position of the left ear	LeftEar	{x1,y1}
The position of the right ear	RightEar	{x2,y2}
The position of the left eye	LeftEye	{x3,y3}
The position of the right eye	RightEye	{x4,y4}
The position of the nose	Nose	{x5,y5}
The position of the left shoulder	LeftShoulder	{x6,y6}
The position of the right shoulder	RightShoulder	{x7,y7}
The position of the midpoint of the left side of the face	LFaceCenter	{x8,y8}
The position of the midpoint of the right side of the face	RFaceCenter	{x9,y9}
The distance from the midpoint of the left side of the face to the left shoulder	Left_face_Shoulder	s1
The distance from the midpoint of the right side of the face to the right shoulder	Right_face_Shoulder	s2
The distance from the left shoulder to the right shoulder	Shoulder_Shoulder	s3

$$x_8 = \frac{x_1\sqrt{(x3-x1}+x2\sqrt{(x5-x3)^2+(y_5-y_3)^2}+x3\sqrt{(x5-x1)^2+(y_5-y_1)^2}}{\sqrt{(x3-x1)^2+(y_3-y_1)^2}+\sqrt{(x5-x3)^2+(y_5-y_3)^2}+\sqrt{(x5-x1)^2+(y_5-y_1)^2}} \quad (1)$$

$$y_8 = \frac{y_1\sqrt{(x3-x1}+y2\sqrt{(x5-x3)^2+(y_5-y_3)^2}+y3\sqrt{(x5-x1)^2+(y_5-y_1)^2}}{\sqrt{(x3-x1)^2+(y_3-y_1)^2}+\sqrt{(x5-x3)^2+(y_5-y_3)^2}+\sqrt{(x5-x1)^2+(y_5-y_1)^2}} \quad (2)$$

Equation (3) represents the value of s_1, Equation (4) represents the value of s_2, and Equation (5) represents the value of .

$$s_1 = \sqrt{(x_6 - x_8)^2 + (y_6 - y_8)^2} \quad (3)$$

$$s_2 = \sqrt{(x_7 - x_9)^2 + (y_7 - y_9)^2} \quad (4)$$

$$s_3 = \sqrt{(x_6 - x_7)^2 + (y_6 - y_7)^2} \quad (5)$$

(2) Calculation of Feature Values

Let feature value 1 be f_1(to exclude the influence of the distance between the subject and the camera, normalization is required), as shown in Equation (6).

$$f_1 = \frac{|(s_1 - s_2) \times 10|}{s_3} \quad (6)$$

Feature value f_1 is used to measure the tendency of the user to lean to the left or right. Based on anatomical observations and experimental results, when the body is not leaning in a seated position, from a frontal perspective, the torso and neck should maintain a relatively stable vertical position, with the body's left and right sides being relatively symmetrical and the head positioned above the centerline. Therefore, when the user maintains good posture, the $f_1$value should be close to 0, indicating that the user's body is not leaning to the left or right.

From experimental results, it can be observed that when the user leans to the left or right, the torso and neck will exhibit a tilting state on one side, causing noticeable displacement of the torso and head relative to the other side. This will cause the f_1 value to deviate from 0, leaning towards the left or right. Specifically, when the user leans to the left or right, the value of f_1 will be larger.

Let feature value 2 be f_2(to exclude the influence of the distance between the subject and the camera, normalization is required), as shown in Equation (7).

$$f_2 = \frac{(s_1 + s_2)}{s_3} \quad (7)$$

This feature value $f_2$is primarily used to determine whether the user exhibits a tendency to hunch or slouch. Based on anatomical observations and experimental results, when the body is in an upright seated position, the torso and neck are in a natural upright state, the angle between the body and the ground is relatively stable, and the head position relative to the shoulders is also normal. Therefore, when the user maintains good posture, the f_2 value should be close to an ideal baseline value, typically between 1.2 and 1.4.

From experimental results, it can be observed that when the user hunches or slouches, the torso and neck will exhibit a certain degree of forward inclination, and the head position relative to the shoulders will be lower. This results in a decrease in the f_2 value, deviating from the baseline value of 1.33. Specifically, when the user hunches or slouches, the $f_2$value may be below 1.1, or even below 0.9.

(3) Error Threshold Analysis

Physiological Differences: There are inherent physiological differences in the human body's structure and form, leading to minor tilting or asymmetry in different individuals when seated. These physiological differences may stem from factors such as skeletal structure, muscle development, body proportions, etc., making it difficult to completely eliminate fluctuations in feature values even in a good seated posture.

Environmental Factors: In real-world usage scenarios, users may be in different environmental conditions, such as different chair heights, desk heights, lighting conditions, etc. These factors may affect the user's posture performance. Even if users try to maintain correct posture, changes in environmental factors may still cause slight fluctuations in feature values.

Postural Adjustments: Users may make minor adjustments to their posture during use, such as slight body rotation or adjusting the comfort of their sitting position. Although these minor postural adjustments do not affect the overall quality of the seated posture, they may lead to slight changes in feature values.

Considering the above factors, it is reasonable to set a certain error range for feature values in practical applications. This error range can tolerate minor variations caused by physiological differences, environmental factors, and postural adjustments, while ensuring the stability of the system and user experience. This design not only reduces false positives but also better adapts to individual differences among users and actual usage environments, thereby improving the reliability and practicality of the system.

3.2.3 Classification based on support vector machine

In this study, we employ the powerful machine learning algorithm of Support Vector Machine (SVM) for target classification. SVM shows significant advantages in addressing problems associated with small datasets, non-linearity (by introducing slack variables), and high-dimensional pattern recognition (through kernel functions). Based on the sample data, an SVM model is constructed, and an appropriate kernel function is selected. The kernel function is shown in Equation (8).

$$k(x_i, x_j) = exp(-\frac{\|x_i - x_j\|^2}{2\sigma^2}) \quad (8)$$

This paper opts for the Gaussian kernel due to its good adaptability and the ability to control model complexity by adjusting the kernel width. The SVM model from the scikit-learn library is used for data training, validation, and testing. First, samples in the training set, validation set, and test set are labeled. Then, using a grid search method, the penalty parameter C and kernel parameter σ^2 are each assigned N and M values, respectively. Different SVMs are trained for each of the N×M combinations of (C,σ^2), and their generalization accuracy is estimated. The combination that yields the highest generalization accuracy among the N×M

combinations of (C, σ^2) is selected as the optimal parameter set. To estimate the generalization accuracy, this paper employs a 5-fold cross-validation method.

4 System Implementation and Testing

4.1 System implementation and results display

Based on the above functional requirements and design plans, we deployed the system on Raspberry Pi hardware. The software developed in this paper was written using PyCharm software. The system interface is shown in Figure 7, enabling the system to receive human target keypoint data and provide intuitive graphical display and posture anomaly identification.

Figure 7 System Interface

For each type of posture including normal sitting posture, hunchback, head tilt to the left, head tilt to the right, body lean to the left, and body lean to the right, the system provides a health assessment. The assessment results are shown in Figure 8: normal sitting posture is labeled as "good" with no voice reminder triggered, while hunchback, head tilt to the left, head tilt to the right, body lean to the left, and body lean to the right are labeled as "bad" with voice reminders triggered.

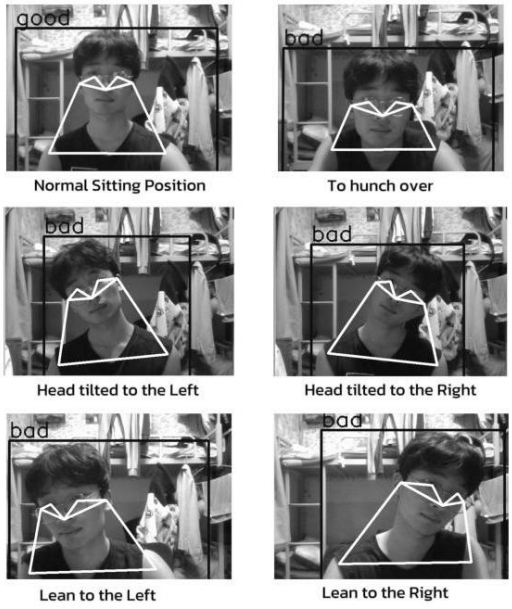

Figure 8 Test Results Diagram

4.2 Testing method and performance estimation

To accurately evaluate the performance of the system in real-world applications, we set up a testing environment that meets the requirements. We positioned the device directly in front of the subject to ensure that the camera can fully capture the upper body of the test subject, with a depth of 1 meter. An example of the setup is shown in Figure 9.

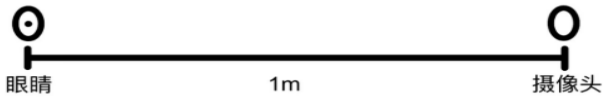

Figure 9 Example Setup for Positioning and Display

We first established criteria to distinguish between different sitting postures, and then conducted health assessments based on these criteria. In the study, we had 10 volunteers (both male and female) sit directly facing the camera and naturally adopt 6 different sitting postures. Each posture needed to be varied continuously, and 100 different images were captured for each posture. In the end, we established the following sitting posture database: including 6 postures, with 100 images for each posture, totaling 6000 images. Through YOLOv8 keypoint extraction, we calculated the f_1 and f_2 values proposed in this paper, and then the SVM classifier made judgments on the health of sitting postures.

For performance evaluation, the data obtained from our volunteers were divided into ten groups per person, and the test results are shown in Table 2. The performance of the SVM classifier is shown in Table 3.

Table 2 Average Feature Values of Volunteers.

Feature Value	Normal Sitting Posture	Hunchback	Head Tilt Left	Head Tilt Right	Body Lean Left	Body Lean Right
f_1	0.031	0.027	1.407	1.361	2.054	1.912
f_2	1.352	0.971	1.191	1.208	1.115	1.186

Table 3 SVM Classifier Test Results.

Index	Recall	Precision
1	0.964	0.964
2	0.929	0.945
3	0.964	0.982
4	0.929	0.945
5	0.964	0.964
6	0.929	0.929
7	0.951	0.982
8	0.975	0.929
9	0.964	0.942
10	0.926	0.934

To validate the overall accuracy of the system's judgments, we invited an additional 10 volunteers for testing. Similarly, each person performed 6 different sitting postures, and 10 frames were captured for each posture. Finally, the accuracy of the judgments was evaluated based on this standard.

Table 4 shows that the detection accuracy based on this standard is relatively high (with an average accuracy of around 95%). Through testing, we found that detecting one frame per second in the actual process is sufficient to meet the requirements. Therefore, this algorithm can basically meet the requirements for accuracy and real-time performance of the sitting posture detection system.

If the judgment method of "if joint in range, good; else, bad" is adopted, the test results are suboptimal due to variations in body proportions among individuals. This stands in stark contrast to the method employed in the previous discussion.

Table 4 Sitting Posture Recognition Rate

Sitting Posture Type	Total Count	Accuracy_svm	Accuracy_In a range
Normal Sitting Posture	100	99%	90%
Hunchback	100	96%	87%
Head Tilt Left	100	94%	91%
Head Tilt Right	100	93%	92%
Body Lean Left	100	92%	89%
Body Lean Right	100	93%	91%

5 Conclusion

This paper proposes a computer vision-based human posture correction system with the aim of correcting poor sitting postures. The camera module v2 combined with YOLOv8 human keypoint detection technology effectively captures the positions of key points on the user's body. The algorithm proposed in this paper preprocesses the position information of human key points into feature values and automatically judges the sitting posture situation based on the SVM method. Experimental results show that the average accuracy of judging 6 types of sitting postures reaches 95%. However, this design has certain limitations; it cannot detect positions arbitrarily. If the human body is not within the range of the camera, the required position information of the human key points cannot be obtained. This limitation is related to the placement of the camera. According to the positioning proposed in this paper, most scene requirements can be fulfilled.

Fund Projects: This work is funded by the Science and Technology Project of Hebei Education Department (No. ZD2022100).

References

[1] Moreira Rayele, et al. A computer vision-based mobile tool for assessing human posture: A validation study[J]. Computer Methods and Programs in Biomedicine, 2022 (214):106565.

[2] Debnath B, O'Brien M, Yamaguchi M, et al. A review of computer vision-based approaches for physical rehabilitation and assessment[J]. Multimedia Systems, 2022,28(1):209-239.

[3] Hellsten T, Karlsson J, Shamsuzzaman M, et al. The potential of computer vision-based marker-less human motion analysis for rehabilitation[J]. Rehabilitation Process and Outcome, 2021(10):1-12.

[4] Andriluka M, Iqbal U, Insafutdinov E, et al. PoseTrack: A benchmark for human pose estimation and tracking[C]. Salt Lake City: IEEE, 2018.

[5] Sun Ke. Hierarchical occlusion reasoning for human pose estimation with incomplete data[J]. IEEE Computer Vision and Pattern Recognition (CVPR), 2021(11):55-59.

[6] Gao Y, Ren Y, Zhang D, et al. Multi-level attention network for fine-grained action recognition[C]. Proceedings of the IEEE/CVF Conference on Computer Vision and Pattern Recognition (CVPR), 2019.

[7] Zhao Y, Xiong Y, Wang L, et al. Weakly supervised action recognition through contrastive spatiotemporal regions[C]. Proceedings of the IEEE/CVF Conference on Computer Vision and Pattern Recognition (CVPR), 2020.

[8] Zhang Y, Cui W, Cao Y, et al. Multimodality human action recognition with deep attention mechanism[J]. Computers & Electrical Engineering, 2020(80):221-239.

[9] Tang Y, Liu R. Skeleton Embedding of multiple granularity attention network for human action recognition[C]. International Conference on Articulated Motion and Deformable Objects Springer, 2020.

[10] Liang ZJ, Wang XL, Huang R, et al. An Expressive deep model for human action parsing from a single image[C]. 2014 IEEE International Conference on Multimedia and Expo (ICME). Chengdu: IEEE, 2014.

[11] Zhai W, Zhang Y, Cheng H, et al. Cooperative eye tracking: a gaze-aware interface for 3D object manipulation[C]. Proceedings of the ACM International Conference on Interactive Surfaces and Spaces, 2019.

[12] Yang X, Chen Y, Liu J, et al. Rapid prototyping of tangible augmented reality interfaces: towards exploratory learning for science education[J]. Interactive Learning Environments, 2019,27(4):469-483.

[13] Zhang D, Peng Y, Yang W, et al. Multi-viewpoint interaction with social robots: a case study of speech therapy for children with autism[J]. Journal of Intelligent & Robotic Systems, 2018,92(3-4):359-372.

[14] Zhang R, Li J, Xiao T, et al. BodyPoseNet: Body pose estimation driven by deep neural networks[J]. Signal Processing: Image Communication, 2021(99):116290.

[15] Chen L, Papandreou G, Kokkinos I, et al. DeepLab: Semantic image segmentation with deep convolutional nets, atrous convolution, and fully connected CRFs[J]. IEEE

Transactions on Pattern Analysis and Machine Intelligence, 2018,40(4):834-848.
[16] Zeng W, Gao Y, Zheng Y, et al. DenseReg: Fully convolutional dense regression for accurate 3D human pose estimation[J]. IEEE Transactions on Image Processing, 2021(30):2830-2842.
[17] Li J, Chen L, Wei Y, et al. CrowdPose: Efficient crowded scenes pose estimation and a new benchmark[C]. Proceedings of the IEEE/CVF Conference on Computer Vision and Pattern Recognition (CVPR), 2019.
[18] Du W, Wang X, Wang X, et al. PoseFix: Model-agnostic general human pose refinement network[C]. Proceedings of the ACM SIGGRAPH Conference on Computer Graphics and Interactive Techniques, 2020.
[19] Zhu L, Zhou C, Li S, et al. CTSegNet: A context-transformed segmentation network for brain tumor segmentation[C]. Proceedings of the IEEE International Conference on Bioinformatics and Biomedicine, 2019.
[20] Ji Xiaodong, Yang Qiaoning, Yang Xiuhui, et al. Human pose estimation: multi-stage network based on HRNet [J]. Journal of Physics: Conference Series, 2022,(1):2400.
[21] He K, Zhang X, Ren S, et al. Spatial pyramid pooling in deep convolutional networks for visual recognition[J]. IEEE Transactions on Pattern Analysis and Machine Intelligence, 2015,37(9):1904-1916.
[22] Papandreou G, Zhu T, Kanazawa N, et al. Towards accurate multi-person pose estimation in the wild[C]. Proceedings of the IEEE Conference on Computer Vision and Pattern Recognition (CVPR), 2017.
[23] Wei L, Zhang S, Dai J, et al. ST-GCN: Spatial temporal graph convolutional networks for skeleton-based action recognition[C]. Proceedings of the IEEE Conference on Computer Vision and Pattern Recognition (CVPR), 2018.
[24] Sun M, He X, Yang S. U^2-Net (RE) for Human Pose Estimation[J]. arXiv preprint arXiv, 2021(2102):380.
[25] Zhou F, Zhu M, Bai J, et al. Deformable ConvNets v2: More deformable, better results[C]. Proceedings of the IEEE/CVF Conference on Computer Vision and Pattern Recognition (CVPR), 2018.
[26] Carreira J, Agrawal P, Fragkiadaki K, et al. Associative embedding: End-to-end learning for joint detection and grouping[C]. Proceedings of the IEEE Conference on Computer Vision and Pattern Recognition, 2016.
[27] Papandreou G, Zhu T, Kanazawa N, et al. PersonLab: Person pose estimation and instance segmentation with a bottom-up, part-based, geometric embedding model[C]. Proceedings of the European Conference on Computer Vision, 2018.
[28] Kreiss S, Bertoni A, Alahi A. PifPaf: Composite fields for human pose estimation[C]. Proceedings of the IEEE Conference on Computer Vision and Pattern Recognition, 2019.
[29] Insafutdinov M, Pishchulin L, Andres B, et al. DeepCut: Joint subset partition and labeling for multi person pose estimation[C]. Proceedings of the IEEE Conference on Computer Vision and Pattern Recognition, 2016.
[30] Newell A, Yang K, Deng J. Stacked hourglass networks for human pose estimation[C]. Proceedings of the European Conference on Computer Vision (ECCV), 2016.
[31] Chen Y, Wang Z, Peng Y, et al. Cascaded pyramid network for multi-person pose estimation[C]. Proceedings of the IEEE Conference on Computer Vision and Pattern Recognition (CVPR), 2018.
[32] Sun K, Xiao B, Liu D, et al. Deep high-resolution representation learning for human pose estimation[C]. Proceedings of the IEEE Conference on Computer Vision and Pattern Recognition (CVPR), 2019.
[33] Xiao B, Wu H, Wei Y. Simple baseline for human pose estimation and tracking[C]. Proceedings of the European Conference on Computer Vision (ECCV), 2018.
[34] Wei L, Zhang S, Yin W, et al. Convolutional pose machines[C]. Proceedings of the IEEE Conference on Computer Vision and Pattern Recognition (CVPR), 2016.

Viser Technology Pte. Ltd.
Mechanical Engineering Science
DOI: 10.33142/mes.v6i1.13222

Research Article Open Access

Research on the Resistance of Cutting Mechanism of Mining Longitudinal Roadheader

Mengjiao NIU, Yong ZHAO, Yongliang YUAN*

He'nan Polytechnic University, Jiaozuo, He'nan, 454000, China

***Corresponding Author:** Yongliang YUAN, E-mail: yuan-yong-liang@163.com*

Abstract

In order to accurately obtain the dynamic characteristics of the cutting mechanism of the mining longitudinal roadheader, combined with the working principle of the mining longitudinal roadheader, the theoretical analysis and derivation are carried out in detail. By using ADAMS to simulate, the resistance curve and torque curve of the cutting mechanism in different directions are obtained. The results show that ADAMS can effectively predict the excavation resistance and torque of the cutting mechanism of mining longitudinal roadheader, which has certain reference value for future optimization design.

Keywords: *longitudinal roadheader; cutting mechanism; dynamic characteristics; dynamics*

1 Introduction

The longitudinal axis roadheader is a pivotal machine in the domain of underground mining, particularly in the extraction of coal reserves [1]. As the mining industry experiences rapid technological advancements and heightened safety regulations, the demand for optimized mining machinery becomes increasingly critical [2-5]. This optimization is essential not only for enhancing productivity but also for ensuring the safety and reliability of mining operations. Central to this optimization process is a comprehensive understanding of the dynamic characteristics of the cutting mechanism within longitudinal axis roadheaders [6].

The dynamic characteristics of the cutting mechanism are crucial as they directly influence the operational efficiency and lifespan of the roadheader [7]. The cutting mechanism operates in a highly dynamic environment, where it is subjected to a variety of forces and torques that can significantly affect the performance and durability of the machine [8-10]. Understanding these dynamic forces and their interactions is key to innovating design and optimization strategies that can lead to reduced operational costs, minimized downtime, and improved safety standards for mining personnel [11].

Previous research has extensively examined various aspects of longitudinal axis roadheaders, including rotary table dynamics, kinematic analysis, and static force evaluation [12]. These studies have provided valuable insights into the geometric design, material selection, and other critical parameters of roadheaders [13-16]. However, there remains a notable gap in the literature regarding the dynamic characteristics of the cutting mechanism [17]. This gap is significant because the dynamic response of the cutting mechanism is essential for determining the overall efficiency and reliability of the roadheader.

This paper aims to address this gap by combining detailed theoretical analyses with advanced simulation methodologies. Utilizing the capabilities of sophisticated mechanical dynamics simulation software, such as ADAMS, this study investigates the resistance and torque profiles of the cutting mechanism under various operational scenarios [18]. The theoretical framework established in this research provides a foundation for understanding the fundamental principles of the cutting process, while the simulation results offer practical insights into the real-world performance dynamics of the cutting mechanism.

The objectives of this study are twofold: to accurately predict the dynamic characteristics of the cutting mechanism and to provide guidance for future structural design and performance optimization efforts. Achieving these objectives is expected to pave the way for a new generation of more efficient, reliable, and safe longitudinal axis roadheaders. This aligns with the broader goals of the coal mining industry, which strives for continuous improvement and innovation in pursuit of operational excellence and sustainability.

Through a combination of theoretical insights and practical simulations, this research aims to deepen the

Received on May 2, 2024; Accepted on June 8, 2024

understanding of the dynamic behaviors of cutting mechanisms in roadheaders. This enhanced understanding is anticipated to drive future innovations in roadheader design, resulting in machines that are not only more efficient and reliable but also safer for operators and more sustainable evolution of mining machinery, reinforcing the commitment to operational excellence and safety in underground mining operations.

2 System Composition and Working Principle

2.1 The cutting mechanism of the mining longitudinal roadheader

The cutting mechanism of the mining longitudinal roadheader is a crucial piece of equipment used in underground mining, particularly suitable for coal mining operations. This machine is composed of multiple core components, each playing a vital role in the overall functionality of the roadheader. The main components include the walking mechanism, loading mechanism, rotating mechanism, and cutting mechanism. These mechanisms work together to achieve efficient coal mining, transportation, and loading tasks [19].

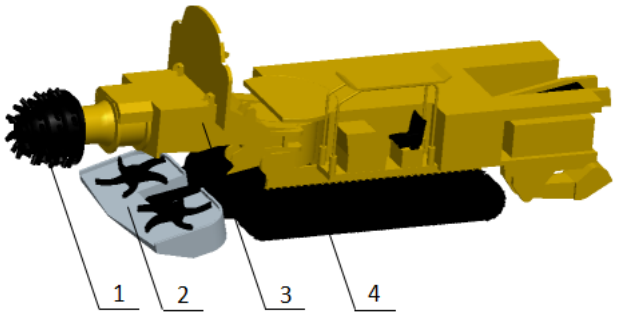

1.Cutting Mechanism; 2. Loading Mechanism; 3. Rotating Mechanism; 4. Walking Mechanism

Figure 1 Schematic Diagram of the System Structure of Vertical-axis roadheader cutting mechanism

Its working principle primarily relies on the combined action of the cutting mechanism and rotating mechanism to extract coal [20-22]. The loading mechanism then transfers the coal particles to the conveyor belt of the mining roadheader. Driven by the machine's drive system, the conveyor belt continuously transports the coal backward, ensuring uninterrupted operation in the cutting area. As the conveyor belt moves the coal to the rear of the roadheader, the coal is either directly loaded into transportation equipment or placed onto a secondary conveyor system for further transport to the surface or processing facilities. Under the action of the walking device, the mining longitudinal roadheader moves forward to the next position and begins mining again. Throughout this process, the mining longitudinal roadheader can operate precisely and efficiently, ensuring minimal downtime and maximum coal extraction. The combination of the cutting, rotating, loading, and walking mechanisms allows the roadheader to function as an integrated unit, significantly improving the overall efficiency and productivity of underground coal mining operations [23]. The schematic diagram of its structure is shown in Figure 1.

2.2 ADAMS

ADAMS (Automatic Dynamic Analysis of Mechanical Systems) is a widely used simulation software for analyzing the dynamics of mechanical systems. It enables engineers to study the complex interactions between different components within a machine, predict the behavior of the system under various conditions, and optimize the design for improved performance.

In this study, ADAMS was utilized to model the cutting mechanism of the vertical-axis shearer. The model included the geometric details of the cutting head, the arrangement of cutting teeth, and the driving mechanism. Constraints and drivers were added to simulate the realistic motion of the cutting mechanism. By applying the appropriate forces and torques, the dynamic simulation provided insights into the resistance and torque characteristics of the cutting mechanism. The results obtained from ADAMS simulations, such as the force and torque curves, were analyzed to understand the dynamic behavior of the cutting mechanism under various operational scenarios. These results are critical for identifying potential areas for design improvement and optimizing the performance of the vertical-axis shearer.

In summary, ADAMS proved to be an effective tool for predicting the dynamic characteristics of the cutting mechanism in mining roadheaders. The insights gained from the simulations have significant implications for the design and optimization of more efficient, reliable, and safe mining machinery.

3 Cutting Mechanism Theoretical Analysis

The cutting mechanism is one of the core components of the vertical-axis shearer, and its primary function is coal mining. In the cutting mechanism, a circle of cutting teeth is typically spiral arranged on the cutting head body [24]. Under the action of the driving device, the cutting head drives the cutting teeth to rotate at high speed, thus mining the hard coal [25]. When cutting coal, the force acting on the cutting teeth is expressed as:

$$Z_0 = A\frac{\left(0.35b_p + 0.3\right)}{b_p + 0.45h + 2.3k_\varphi} htk_z k_\phi k_y k_c k_{ot} \frac{1}{\cos\beta} \quad (1)$$

Where, A represents the average cutting impedance when each stratum pressure exists, measured in N/mm;

b_p is the working width of the cutting tooth, measured in mm; h is the average mining thickness, also measured in mm; k_φ is the coal brittleness and plasticity impact coefficient; k_z is the surface impact coefficient; k_ϕ is the blade impact coefficient; k_y is the cutting ratio impact coefficient; k_c is the mining impact coefficient; k_{ot} is the underground pressure impact coefficient; β represents the installation angle of the cutting tooth.

For a cutting tooth that has been dulled due to prolonged use, its cutting resistance can be expressed as:

$$Z = Z_0 + \mu_d \sigma_y \left(0.85 S_j + k_\sigma\right) \tag{2}$$

Where, μ_d represents the cutting motion resistance coefficient; σ_y is the compressive strength, measured in MPa; S_j is the area of the cutting tooth after dulling in the traction direction, measured in mm²; k_σ is the coal compression coefficient.

Establishing a coordinate system with the forward direction of the vertical-axis shearer as the Z-axis and the vertical motion direction as the X-axis, the forces acting on the cutting head of the cutting mechanism can be obtained in the XYZ directions:

$$F_x = -Y_i \cos\alpha + Z_i \sin\alpha \tag{3}$$

$$F_y = -Y_i \sin\alpha + Z_i \cos\alpha \tag{4}$$

$$F_z = X_i \tag{5}$$

Where, X_i, Y_i, Z_i represent the axial force, radial force, and tangential force, respectively, acting on the cutting tooth; α represents the angle between the cutting tooth and the X-axis direction.

4 Simulation Calculation

The established model is imported into ADAMS. Constraints and drivers are added to the model according to actual conditions. In order to obtain the dynamic performance of the vertical-axis shearer, the GSTIFF solver is selected to simulate and solve the model. The simulation results of the cutting mechanism are shown in Figures 2-5.

According to Figure 2, the maximum force acting on the cutting head is 187.54 kN. The fluctuation of forces on the cutting head is significant, primarily due to the discrete contact between the cutting head and the coal. Figure 3 indicates that the total external force gradually increases from 0 as the cutting mechanism operates. The overall trend of the total external force remains relatively stable during the operation of the cutting mechanism, consistent with actual working conditions. This stability is mainly attributed to the fact that once the cutting head fully enters the coal, the variation in cutting resistance is relatively small.

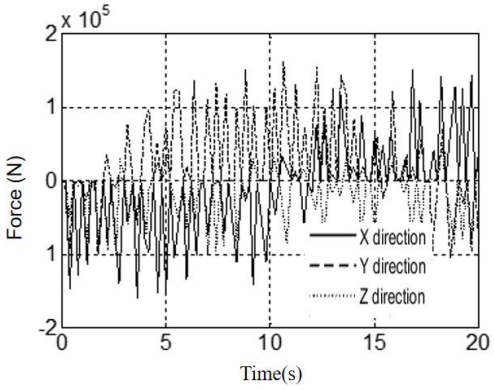

Figure 2 Force Curve of the Cutting Hea

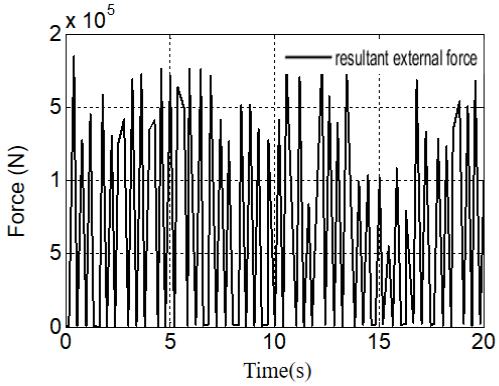

Figure 3 Time-dependent Curve of External Forces

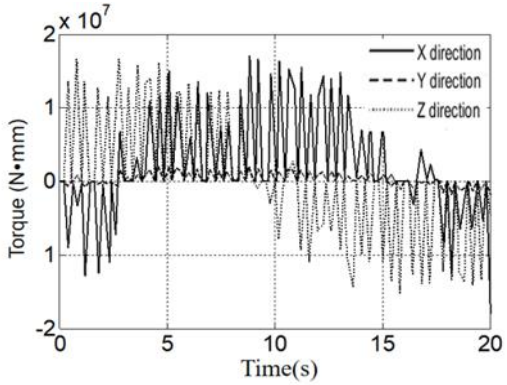

Figure 4 Torque Curve of the Cutting Head

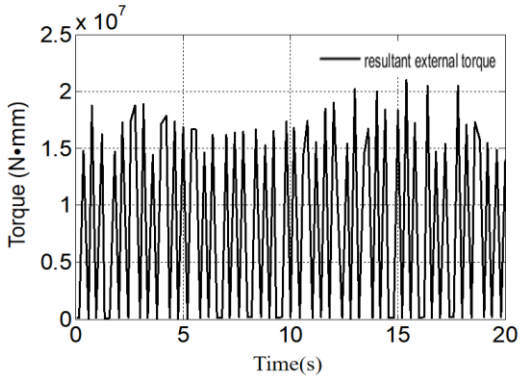

Figure 5 Time-dependent Curve of Total External Force Moment

From Figures 4 and 5, it can be observed that both the cutting resistance torque and the total external force torque vary with the load, with alternating peaks in torque acting on the cutting head. This indicates that the cutting head of the vertical-axis shearer experiences uneven forces during operation, accompanied by the generation of vibrations. Therefore, there is significant room for optimization in the design of the cutting head to improve its lifespan.

5 Conclusion

In conclusion, this study conducted a comprehensive analysis of the dynamic characteristics of the cutting mechanism of the vertical-axis shearer. Through theoretical analysis, the resistance equation of the cutting head was derived, providing insights into the forces and torques acting on the cutting mechanism during operation. Subsequently, utilizing ADAMS dynamic simulation software, the resistance curve and torque curve of the cutting head were obtained, offering a detailed understanding of its dynamic behavior under various operating conditions.

The results of the simulation demonstrate the effectiveness of ADAMS in predicting the dynamic characteristics of complex mechanisms, such as the cutting mechanism of the vertical-axis shearer. This not only enhances our understanding of the machine's performance but also provides a valuable basis for future optimization designs. By accurately predicting the dynamic behavior of the cutting mechanism, manufacturers and engineers can make informed decisions to improve the efficiency, reliability, and safety of longitudinal axis roadheaders.

Moving forward, this research sets the stage for further advancements in the design and performance optimization of mining machinery. By addressing the gap in understanding regarding the dynamic characteristics of the cutting mechanism, this study contributes to the broader goals of enhancing productivity and safety in the coal mining industry. Further studies could explore additional aspects of the longitudinal axis roadheader and its components, ultimately leading to the development of more efficient and reliable mining equipment.

References

[1] Zhang Xin, Zeng Qingliang. Research on Multi-Objective Optimization Design of Shearer Cutting Head [J]. Coal Mine Machinery, 2005,26(6):1-3.

[2] Qiqian Wang. Optimization of the Upward Horizontal Filling Mining Method [J]. Construction Engineering and Management, 2023,5(7):151-153.

[3] Baozhug Ge. Analysis of Common Mining Technologies in Coal Mine Operations [J]. Engineering Construction, 2022,5(11):86-88.

[4] Dong L, Tong X, Li X, et al. Some Developments and New Insights of Environmental Problems and Deep Mining Strategy for Cleaner Production in Mines [J]. Journal of Cleaner Production, 2019(210):1562-1578.

[5] Hodgkinson J H, Smith M H. Climate Change and Sustainability as Drivers for the Next Mining and Metals Boom: The Need for Climate-Smart Mining and Recycling [J]. Resources Policy, 2021(74):101205.

[6] Shi Maolin, Sun Wei, Song Xueguan. Research Progress on Big Data in Tunnel Boring Machines: Data Mining to Boost Tunnel Excavation [J]. Journal of Mechanical Engineering, 2021,57(22):344-358.

[7] Deshmukh S, Raina A K, Murthy V, et al. Roadheader – A Comprehensive Review [J]. Tunnelling and Underground Space Technology, 2020(95):103148.

[8] Shang Yaoxing, Li Yao, Yu Tian, et al. Current Status and Challenges of Lightweight Composite Hydraulic Cylinders [J]. Journal of Mechanical Engineering, 2022,57(24):13-38.

[9] Cheng K, Niu Z C, Wang R C, et al. Smart Cutting Tools and Smart Machining: Development Approaches, and Their Implementation and Application Perspectives [J]. Chinese Journal of Mechanical Engineering, 2017(30):1162-1176.

[10] Krolczyk G M, Maruda R W, Krolczyk J B, et al. Ecological Trends in Machining as a Key Factor in Sustainable Production – A Review [J]. Journal of Cleaner Production, 2019(218):601-615.

[11] Cheng Daxian. Mechanical Design Handbook [M]. Beijing: Chemical Industry Press, 2008.

[12] Feng J, Tian M, Song J, et al. Method for Automatic Control of Cutting Speed of a Longitudinal Roadheader Taking into Consideration the Temperature Load [J]. Russian Physics Journal, 2021(64):1006-1017.

[13] Wang Guofa, Liu Feng, Meng Xiangjun, et al. Research and Practice of Coal Mine Intelligentization (Primary Stage) [J]. Coal Science & Technology, 2019, 47(8):55-58.

[14] Zhu Bin, Wang Jian, Xu Zhuang, et al. Mechanical Mechanism of New Shield Tunneling Underpassing Existing Structures [J]. Journal of Shandong University (Engineering Edition), 2022,52(4):175-182.

[15] Cheluszka P, Remiorz E, Rostami J. The Use of a Roadheader Simulator in Research of Dynamics and Energy-Consumption of Excavating Underground Roadways and Tunnels [J]. Energies, 2022,15(18):6673.

[16] Salmi E F, Phan T, Sellers E J, et al. A Review on the Geotechnical Design and Optimisation of Ultra-Long Ore Passes for Deep Mass Mining [J]. Environmental Earth Sciences, 2024,83(10):301.

[17] Sun Yanfeng, Wang Ying, Ma Ziyun. Research on Cutting Control Method of Shearer [J]. Coal Mine Machinery, 2018,39(9):126-128.

[18] Khaghani A. Investigation of the Smart Tooling System and Dynamics in Ultraprecision Machining of Freeform Surfaces and its Implementation Perspective [D]. Brunel University London, 2020.

[19] Luo Wen. Innovation-Driven Development Status and Experience of Guoneng Shendong Coal Group [J]. Coal Science & Technology, 2023,51(2):22-27.

[20] Alagan N T, Hoier P, Zeman P, et al. Effects of High-Pressure

Cooling on the Flank and Rake Faces of WC Tool on the Tool Wear Mechanism and Process Conditions in Turning of Alloy 718 [J]. Wear, 2019(434):102922.

[21] Song Xuanmin, Zhu Defu, Wang Zhonglun, et al. 40 Years of Comprehensive Mining in China: Research Progress in Theory and Technical Equipment [J]. Coal Science & Technology, 2021,49(3):1-29.

[22] Wang Haijun, Wang Honglei. Status and Prospects of Key Technologies for Intelligent Belt Conveyors [J]. Coal Science & Technology, 2022,50(12):225-239.

[23] Wang Xuecheng. Characteristic Analysis of Cantilever Shearer Cutting Head in Rock Tunnel [J]. Coal Mine Machinery, 2017,38(10):118-120.

[24] Zhang Qiang, Mao Jun, Tian Dafeng. Multi-Objective Fuzzy Reliability Optimization of Shearer Cutting Head Based on Genetic Algorithm [J]. Journal of China Coal Society, 2008,33(12):1435-1437.

[25] Geng Fengxiao. Reliability Research and New Technology Application of Hydraulic Cylinder of Hard Rock Shearer [J]. Coal Mine Machinery, 2018,39(2):109-110.

Viser Technology Pte. Ltd.
Mechanical Engineering Science
DOI: 10.33142/mes.v6i1.13223

Research Article Open Access

Research on the Influence of Raceway Waviness on the Vibration Characteristics of Deep Groove Ball Bearings

Yuanlong CHEN, Jiarui ZHOU, Xinyu WEN, Shaoqi WANYAN, Yuqing WANG*

School of Mechanical Engineering, Hefei University of Technology, Hefei, Anhui, 23009, China

***Corresponding Author:** *Yuqing WANG, E-mail: yuqingw@hfut.edu.cn*

Abstract

The dynamics model of a 2-degree-of-freedom deep groove ball bearing is established by incorporating the raceway surface waviness model comprising multiple sinusoidal functions superposition. The model is solved using the fourth-order Runge-Kutta method to obtain the vibration characteristics including displacement, velocity, acceleration, and frequency of the bearing. Validation of the model is accomplished through comparison with theoretical vibration frequencies. The influence of the amplitude of waviness of the inner and outer ring raceway surfaces of deep groove ball bearings on the vibration displacement, peak-to-peak vibration displacement and root-mean-square vibration acceleration is analyzed, and the results show that as the amplitude of the inner and outer ring raceway surfaces waviness increases, all the vibration characteristic indexes increase, indicating that the vibration amplitude of the bearings as well as the energy of the waviness-induced shock waveforms increase with the increase of the amplitude of the waviness.

Keywords: *Waviness; Deep groove ball bearing; Vibration characteristics; Dynamics*

1 Introduction

The deep groove ball bearing serves as a precise component that converts sliding friction into rolling friction, offering benefits such as increased power transmission efficiency and a low coefficient of friction. This type of bearing is widely employed as a fundamental element in rotating machinery [1-2]. In instances where the raceway surface of deep groove ball bearings exhibits defects, the contact force between the rolling element and raceway of the bearings undergoes non-uniform alterations, leading to irregular vibrations and fatigue-related damage. Consequently, delving into the impact of raceway surface imperfections on the vibration properties of rolling bearings holds substantial importance.

Kankar P. K et al [3] conducted a study focusing on examining the impact of the surface waviness of the bearing raceway on the nonlinear vibration characteristics of a bearing rotor system. The research integrated considerations of nonlinear contact stiffness and nonlinear damping occurring between the rolling body and the raceway to gain insights into the system's vibrational behavior. Shah D S et al [4] introduced the changes in bearing stiffness and damping caused by lubricating oil film, and he took into account the mass of shaft, ring, rolling element and shell in modeling, established a mechanical model of the surface waviness of deep groove ball raceway. Sun M et al. [5] used autocorrelation function to simulate the random surface waviness of inner and outer raceways, established a rolling body-raceway contact model considering the surface waviness, and combined it with the theory of acoustic equations, established the computational model of vibration noise of the rolling body and the inner ring. Yang M H et al [6] introduced a different method to solving the Reynolds equation to investigate the effect of different surface waviness parameters of shaft diameter and shaft tile on the static parameters of dynamic compression shaft diameter bearings on the vibration characteristics of the bearings. Liu J et al [7] proposed an enhanced time-varying displacement excitation model for circularity and waviness by using a combination of several sinusoidal functions and improved the dynamics model in the previous study to take into consideration the vibration noise of the rolling element and inner ring including the effect of coupling errors including roundness and corrugation on the bearing vibration characteristics. Tallian T E and Gustafsson O G [8] proposed a dynamical model considering the waviness and investigated the effect of mass and flexibility attached to the bearing on the vibration characteristics. Choudhury A and Tandon N [9] proposed a dynamical model considering free mode and bending vibration of rolling bearings to study the effect of waviness and roller

Received on March 19, 2024; Accepted on April 11, 2024

size deviation on the frequency of rolling bearings. Nizami A [10] developed a computer program to simulate the degree of waviness on the inner and outer rings of rolling bearing raceways and on the surface of rolling elements, investigated the effects of the number of balls, preload, and the degree of waviness on the vibration characteristics of rolling bearings, and verified the correctness of the model by experimental results.

In summary, the surface defects of rolling bearings can be divided into two categories: local defects and distributed defects. Distributed defects include surface roundness, surface waviness, surface roughness and rolling element size deviation, etc., among which the influence of surface waviness amplitude on the vibration characteristics of bearings is less studied. In this work, a reasonable dynamic model of rolling bearing under the excitation of waviness is established by comprehensively considering the corrugation error of the surface of the raceway of the inner and outer rings of rolling bearings. The dynamic model is solved by the fourth-order Runge-Kutta method, and the solution results are compared with the theoretical frequency value to verify the correctness of the established model. Building on this foundation, the research investigates how the amplitude of raceway surface waviness affects the vibration characteristics of rolling bearings.

2 Theoretical Modeling

Different from previous studies, a sinusoidal basis was introduced in this work to characterize the surface waviness of inner and outer raceways, so as to accurately characterize the surface characteristics of inner and outer raceways of rolling bearings under actual working conditions. In contrast to the traditional theoretical research based on the ideal raceway surface model, this work takes the spatial variable curvature surface of the inner and outer raceway and the spatial variable curvature contact surface between the rolling element and the raceway as the starting point, and establishes the theoretical model of surface waviness as shown in Figure 1.

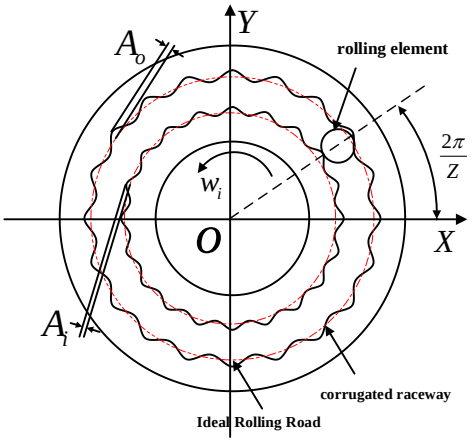

Figure 1 Schematic diagram of sinusoidal basis model of raceway waviness in inner and outer rings

First, the mechanical equations of bearing vibration induced when each roller contacts the outer raceway surface waviness are characterized:

$$T_o = \sum_{s=1}^{k} A_{os} \sin(N_{os}\theta_j + \varphi_{os}) \tag{1}$$

Where A_{os}, N_{os} and φ_{os} denote: the maximum magnitude of the s-order waveform, the wave number, and the initial phase angle, respectively. In addition, the contact angle θ_j between the s-th rolling element and the raceway satisfies the following constraints:

$$\theta_j = \begin{cases} \frac{2\pi}{Z}(j-1) + \omega_c t + \varphi_{0x} & inner \quad ring \\ \frac{2\pi}{Z}(j-1) + (\omega_c - \omega_i)t + \varphi_{0x} & outer \quad ring \end{cases} \tag{2}$$

Where j, Z, w_c, φ_{0x} and w_i denote: the j-th rolling element, the total number of rolling elements, the cage angular velocity, the position angle of the first rolling element relative to the x-axis, and the angular velocity of the inner ring.

By substituting equation (2) into equation (1), the expression of outer ring waviness can be obtained:

$$T_o = \sum_{s=1}^{k} A_{os} \sin\left\{ N_{os}\left[\frac{2\pi}{Z}(j-1) + \omega_c t + \varphi_{ox} \right] + \varphi_{os} \right\} \tag{3}$$

Similarly, the inner ring waviness is characterized as:

$$T_i = \sum_{s=1}^{k} A_{is} \sin\left\{ N_{is}\left[\frac{2\pi}{Z}(j-1) + (w_c - w_i)t + \varphi_{0x} \right] + \varphi_{is} \right\} \tag{4}$$

Secondly, this paper proposes a spring-mass-damping model for rolling bearings by comprehensively considering the change of contact stiffness under the influence of bearing mass, damping and corrugation degree. Figure 2 represents the established dynamic model of deep groove ball bearing. In order to facilitate numerical analysis, the rolling element is uniformly distributed, and the contact between the raceway and the rolling element follows the Hertzian contact theory [11], then the contact between the rolling element and the inner and outer rings is regarded as circular point contacts. Support the plane passing through the center of the rolling body and parallel to the axial plane be the I main plane, and the plane passing through the center of the rolling body and perpendicular to the I main plane be the II main plane, and the contact stiffness K between the raceway and the rolling body can be expressed as:

$$K = \left(\frac{\pi^2 k^2 E^{*2} \Sigma}{4.5 \Gamma^3 \Sigma \rho} \right)^{0.5} \tag{5}$$

Where E^*, $\Sigma\rho$ and k denote: equivalent modulus of elasticity, contact surface curvature sum and elliptic parameters. Moreover, for the full elliptic integrals of

classes I and II Λ and M satisfying:

$$\frac{2}{E^*}=\frac{1-\mu_1^2}{E_1}+\frac{1-\mu_2^2}{E_2} \tag{6}$$

Where $E_1(E_2)$, $u_1(u_2)$ and $\Sigma\rho_I(\Sigma\rho_{II})$ denote: the sum of the modulus of elasticity of the rolling body(raceway) material, the Poisson ratio of the rolling body(raceway) material, and the curvature of the I(II) principal plane.

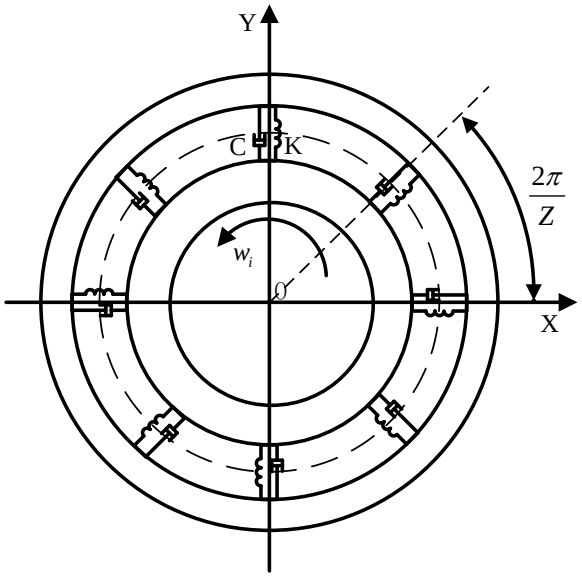

Figure 2 Schematic diagram of the dynamic model of a deep groove ball bearing

Subsequently, the raceway surface in contact with the rolling element is modeled as shown below:

$$\begin{cases} k=1.0339ln\left(\dfrac{\sum\rho_I}{\sum\rho_{II}}\right)^{0.6360} \\ \Lambda=1.5277+0.6023ln\left(\dfrac{\sum\rho_I}{\sum\rho_{II}}\right) \\ M=1.0003+0.5968\left(\dfrac{\sum\rho_{II}}{\sum\rho_I}\right) \end{cases} \tag{7}$$

By integrating equations (5) through (7), one can derive the comprehensive contact stiffness encompassing the interaction between the rolling body and both the inner and outer rings:

$$K=\left(\frac{1}{K_i^n}+\frac{1}{K_o^n}\right)^{-n} \tag{8}$$

Where K_i and K_o denote the contact stiffness of the rolling element with the inner and outer rings. In addition, the deep groove ball bearing load-deflection coefficient n considered in this work is 1.5.

Finally, in view of the rolling bearing operation, the raceway is prone to displacement and deformation of the actual working conditions, the total contact deformation δ_j can be expressed as:

$$\delta_j=x\cos\theta_j+y\sin\theta_j-\gamma+T_i+T_o \tag{9}$$

Where $x(y)$ and γ is the displacement and radial clearance of the inner ring in the $X(Y)$ direction. The contact coefficient S_j is introduced to characterize the difference between the loaded and unloaded areas of the raceway:

$$S_j=\begin{cases}1, & \delta_j>0\\ 0, & \delta_j\le 0\end{cases} \tag{10}$$

Development of a two-degree-of-freedom rolling bearing dynamics model to describe bearing vibration characteristics under waviness excitation:

$$\begin{cases} m\ddot{x}+c\dot{x}+\sum_{j=1}^{z}KS_j(x\cos\theta_j+y\sin\theta_j-\gamma+T_i+T_o)^n\cos\theta_j=F_x \\ m\ddot{y}+c\dot{y}+\sum_{j=1}^{z}KS_j(x\cos\theta_j+y\sin\theta_j-\gamma+T_i+T_o)^n\sin\theta_j=F_y \end{cases} \tag{11}$$

Where m, c and $F_x(F_y)$ denote: the mass of the inner ring and the supporting shaft, the internal damping coefficient of the bearing, and the radial force of the bearing in the direction of the $X(Y)$ axis.

3 Numerical Algorithm

Based on equations (1)-(11), this work takes deep groove ball bearing 6308 as the entry point to analyze the influence mechanism of raceway waviness degree on bearing vibration characteristics. Its basic geometric parameters are shown in Table 1.

Table 1 Geometric dimensions of 6308 deep groove ball bearings

Physical parameter	Operator	Dimension	Value
Inner ring diameter	D_{in}	mm	40
Diameter of outer ring	D_{out}	mm	90
Rolling body pitch diameter	D	mm	65
Number of scrollers	Z	\	8
Contact angle	θ	°	0
Rolling body diameter	d	mm	15.081
Inner ring raceway diameter	D_i	mm	80.088
Outer ring raceway diameter	D_o	mm	49.912

Take the mass of the inner ring of the rolling bearing $m=0.6kg$, damping coefficient $c=200Ns\cdot m^{-1}$ and bearing speed $N_s=2000r\cdot\min^{-1}$. Solve the dynamics equation of equation (13) using the fourth-order Runge-Kutta method with a time step $\Delta t=5\times10^{-6}s$. It's assumed that the initial displacement of the system $x_0=y_0=10^{-6}m$ and the initial velocity $\dot{x}_0=\dot{y}_0=0$. The corresponding algorithmic flowchart for numerical computation is shown in Figure 3.

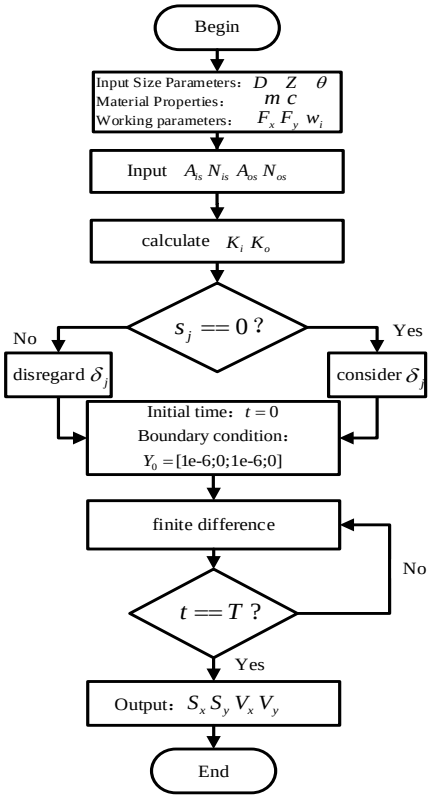

Figuer 3 Algorithm flowchart

4 Vibration Characterization Analysis

4.1 Solution of dynamic equations

In this paper, the basic size parameters, initial load and speed of the rolling bearing are input first. Secondly, according to the established waviness model, input parameters such as the amplitude and wave number of the raceway waviness. Then, the contact stiffness between the rolling element and the inner and outer rings of the raceway is calculated. Finally, the four-order Runge-Kutta method was used to calculate the dynamics model of 2 degrees of freedom. At the end of the iteration, the displacement, velocity and acceleration curves of the inner ring of the rolling bearing on the x and y axes were output, as shown in Figure 4.

4.2 Model verification

4.2.1 Verification of vibration characterization

The displacement curves along the x-axis and y-axis were subjected to Fourier transformation to generate the displacement frequency domain representation of the bearing in both the x-axis and y-axis orientations, as illustrated in Figure 5.

The results presented in Figure 4 (a) - (f) indicate a noticeable periodicity in the vibration displacement, velocity, and acceleration of the inner ring of the rolling bearing in the time domain waveform. This behavior is attributed to the alternating odd and even number of balls in the load region of the ball bearing under radial force influence, leading to vibrations of the bearing with the outer ring at specific frequencies. Further observation of Figure 5 shows that the inner ring of the bearing in the x-axis direction and the y-axis direction are in the 103.3Hz at the obvious peak, and the corresponding conditions listed in Table 2 of the ball bearing outer ring through the frequency of 102.4Hz is basically consistent with the establishment of the model is correct.

Table 2 6308 deep groove ball bearings at various frequencies at $2000r \cdot \min^{-1}$

Rolling body rotation frequency f_{bs}	Cage rotation frequency f_c	Outer Ring Passing Frequency f_{bpo}	Inner Circle Passing Frequency f_{bpi}
70.0Hz	12.8Hz	102.4Hz	164.3Hz

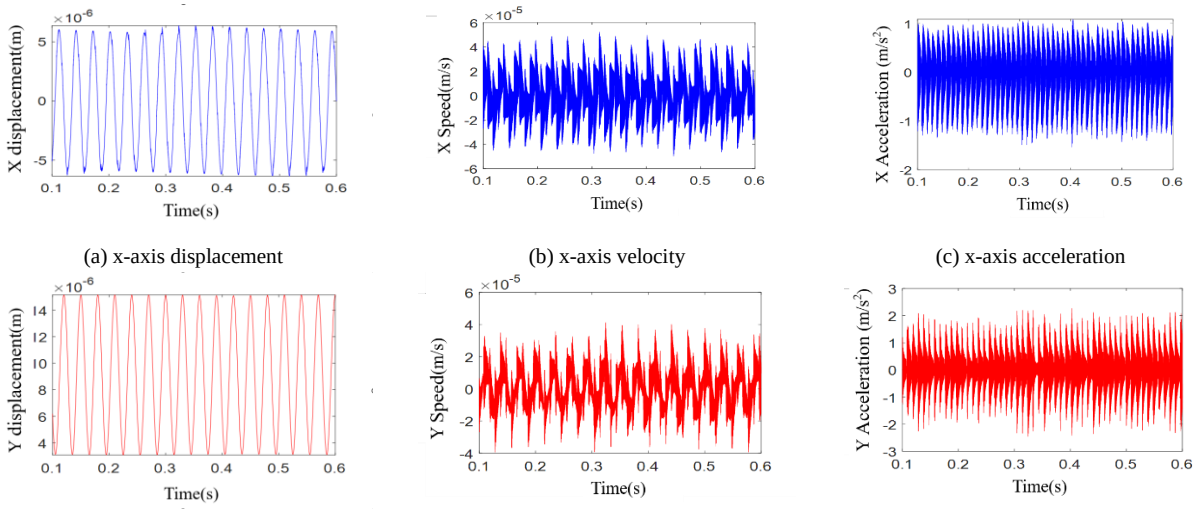

(a) x-axis displacement (b) x-axis velocity (c) x-axis acceleration

(d) y-axis displacement (e) y-axis velocity (f) y-axis acceleration

Figure 4 Vibration displacement, velocity and acceleration curves of the inner ring of the bearing

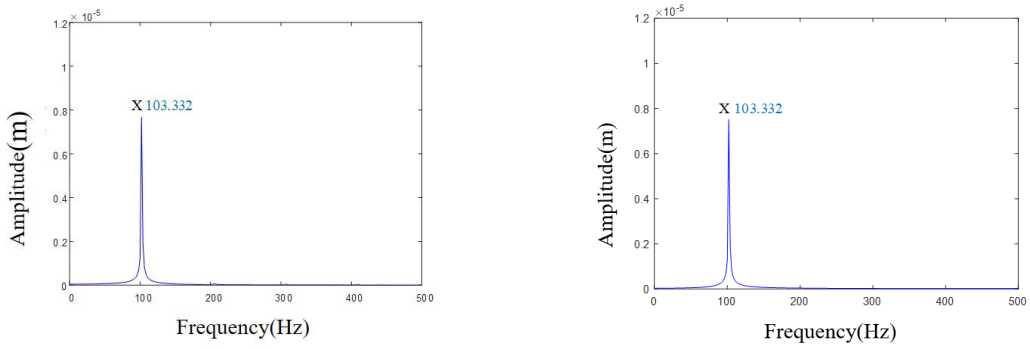

(a) x-axis direction (b) y-axis direction

Figure 5 Spectrogram of vibration displacement of the inner ring of the bearing

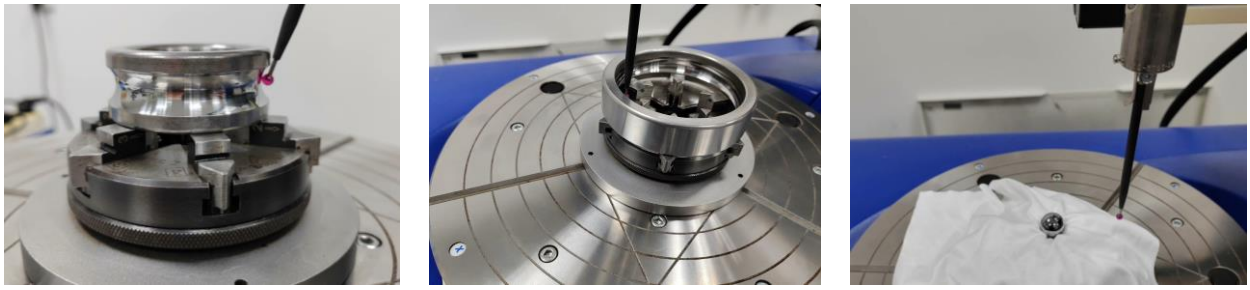

(a) internal raceway (b) outer raceway (c) rolling element

Figure 6 Waviness measurement of 6308 deep groove ball bearing

4.2.2 Verification of waviness model

The waviness model proposed in this study is a composite of sine functions with varying amplitudes and wave numbers. To validate the accuracy of the established model, a waviness test was conducted on a 6308 deep groove ball bearing using an MMD-100JS profilometer. The measurement points are illustrated in Figure 6.In order to ensure accuracy in the measurement test, three measurements were conducted for each part, and the average value of the three measurement results was utilized for data analysis. Taking the waviness of the inner raceway surface as an example, this data was analyzed.

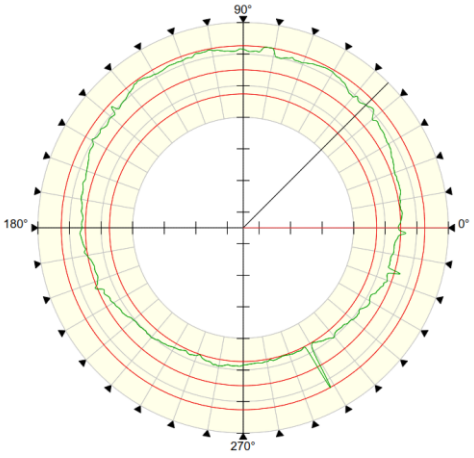

Figure 7 Waviness error diagram of the inner ring

The computer system employs the minimum region method for roundness error calibration to evaluate and present the measurement results graphically, as depicted in Figure 7.

Harmonic analysis of the measurement results, take 4-100upr data, get 6308 deep groove ball bearing inner ring raceway waviness error of the harmonic analysis of the data as Table 3, Figure 8 shows.

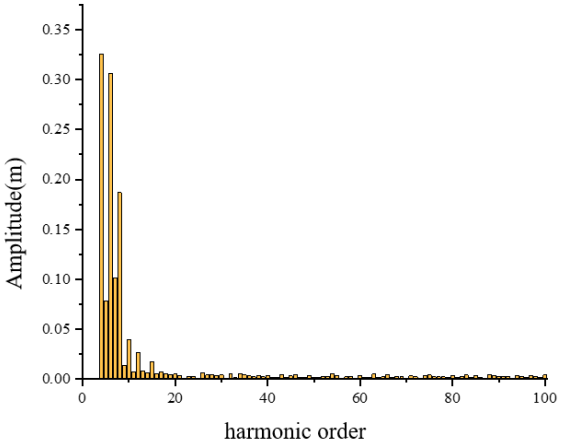

Figure 8 Histogram of waviness harmonic analysis of inner ring

The results of the harmonic analysis reveal that the waviness of the inner ring in the rolling bearing is formed through the superposition of sine functions with varying amplitude and frequency. This finding aligns with the established waviness model, thereby confirming its accuracy.

Table 3 Inner raceway harmonic analysis data (4-100upr)

UPR	N+0	N+1	N+2	N+3	N+4	N+5	N+6	N+7	N+8	N+9
0				0.3256	0.0784	0.3065	0.1012	0.1869	0.014	0.0394
10	0.0075	0.0271	0.0085	0.0065	0.0178	0.0052	0.007	0.0057	0.0045	0.005
20	0.0036	0.0006	0.0028	0.0027	0.0012	0.0065	0.0045	0.0049	0.0037	0.0045
30	0.0009	0.0055	0.0018	0.0057	0.0043	0.0033	0.0023	0.004	0.0024	0.0038
40	0.0018	0.0022	0.0046	0.0019	0.0033	0.0044	0.0017	0.0016	0.004	0.0014
50	0.0021	0.0029	0.0024	0.0052	0.0038	0.0004	0.0023	0.003	0.0009	0.0033
60	0.0018	0.0019	0.0053	0.0019	0.0025	0.0046	0.0022	0.003	0.0031	0.001
70	0.0034	0.0025	0.0011	0.0039	0.0044	0.0025	0.0024	0.0023	0.0019	0.0041
80	0.0022	0.0025	0.0043	0.0017	0.0039	0.0021	0.0013	0.0042	0.0035	0.0029
90	0.0029	0.003	0.0011	0.0036	0.0026	0.0022	0.0035	0.0027	0.0022	0.0043

4.3 Influence of waviness amplitude on vibration characteristics of deep groove ball bearings

Taking the bearing radial load $F_x = 0$, $F_y = 20N$, radial clearance $C_y = 1um$, waviness number 7, and bearing speed $N_s = 2000r \cdot \min^{-1}$ as the working condition, the influence of raceway surface waviness amplitude on bearing vibration displacement, peak-to-peak value of vibration displacement and root mean square value of acceleration was analyzed.

4.3.1 Inner ring

The vibration displacement curve of the bearing in the y-axis direction is shown in Figure 9 when the inner ring ripple amplitude is 0.2um, 0.4um, 0.8um and 1.2um. From Figure 9, it can be seen that the vibration displacement of the rolling bearing in the y-axis direction increases with the increase of the amplitude of the inner ring waviness. The relationship between the inner ring waviness amplitude and the peak-to-peak value of the bearing vibration displacement in the y-axis direction is shown in Figure 10. Analysis of Figure 10 reveals a direct relationship between the peak-to-peak value of the vibration displacement in the y-axis direction of the bearing and the inner ring waviness amplitude, indicating that the former increases proportionally with the latter.

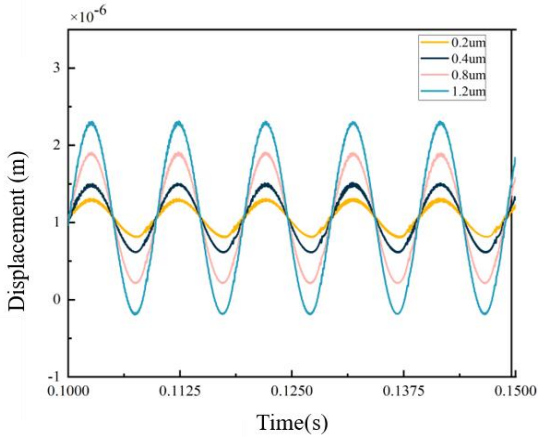

Figure 9 The influence of the waviness amplitude of the inner ring on the vibration displacement in the y-axis direction of the bearing

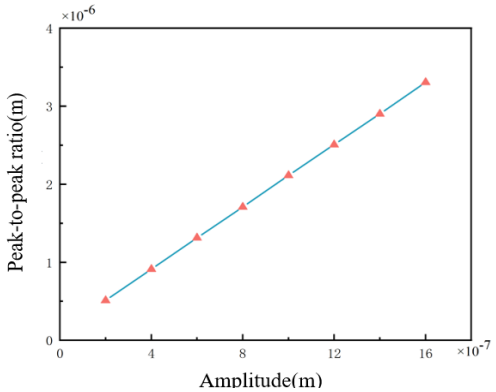

Figure 10 The influence of the waviness amplitude of the inner ring on the vibration displacement in the y-axis direction of the bearing

Root mean square (RMS), referred to as the root mean square or effective value [12], is commonly used to represent the effective value of a physical quantity. In this paper, the RMS value of the vibration acceleration of the bearing is used to represent the energy of the impact waveform induced by waviness, and its expression is as follows:

$$RMS_a = \sqrt{\frac{1}{N}\sum_{i=1}^{N} a_i^2} \tag{14}$$

Where a_i denote the i-th acceleration data, N denotes the total number of acceleration data to be analyzed

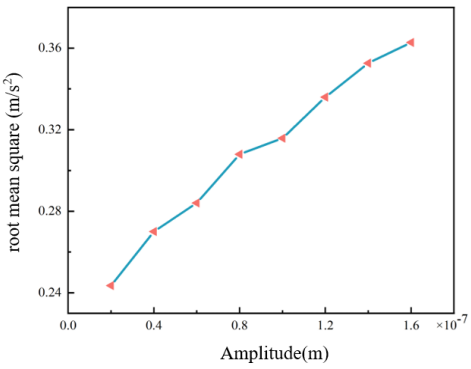

Figure 11 The effect of the waviness amplitude of the inner ring on the RMS value of vibration acceleration in the y-axis direction of the bearing

Figure 11 depicts the correlation between the amplitude of inner ring waviness and the root mean square (RMS) value of vibration acceleration along the y-axis of the bearing. The graphical suggests a direct relationship between the vibration acceleration's RMS value in the bearing shaft direction and the inner ring waviness amplitude. As the amplitude of inner ring waviness escalates, the RMS value of vibration acceleration also rises, indicating a corresponding increase in the impact waveform energy caused by the waviness.

4.3.2 Outer ring

The vibration displacement curve of the bearing in the y-axis direction is depicted in Figure 12 for varying amplitudes of outer ring waviness, specifically at 0.2um, 0.4um, 0.8um and 1.2um. Analysis of Figure 12 reveals a direct correlation between the amplitude of the outer ring waviness and the vibration displacement of the rolling bearing along the y-axis direction, indicating that as the outer ring waviness amplitude increases, so does the vibration displacement.

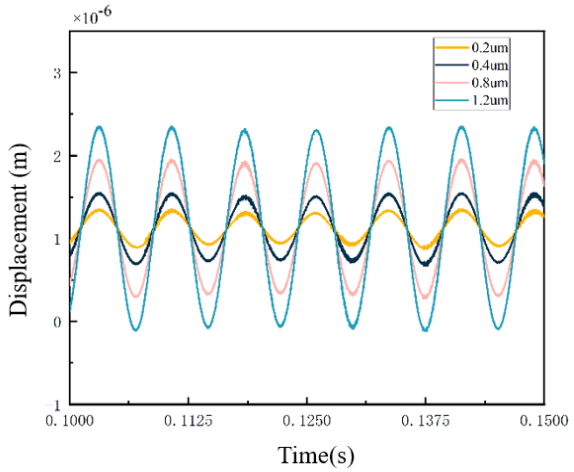

Figure 12 The influence of the waviness amplitude of the outer ring on the vibration displacement in the y-axis direction of the bearing

The relationship between the outer ring waviness amplitude and the peak-to-peak value of vibration displacement in the y-axis direction of the bearing is shown in Figure 13. From Figure 13, it can be seen that the peak-to-peak value of the vibration displacement of the bearing in the y-axis direction is positively correlated with the magnitude of the outer ring waviness, and the peak-to-peak value of the vibration displacement in the y-axis direction of the bearing increases with the increase in the magnitude of the outer ring waviness. The relationship between the outer ring waviness amplitude and the root-mean-square value of the vibration acceleration in the y-axis direction of the bearing is shown in Figure 14. It can be seen from Figure 14 that the RMS value of the vibration acceleration in the y-axis direction of the bearing is positively correlated with the amplitude of the outer ring waviness and increases with the increase of the amplitude of the outer ring waviness, indicating that with the increase of the amplitude of the outer ring waviness, the energy of shock waveforms triggered by the waviness increases subsequently.

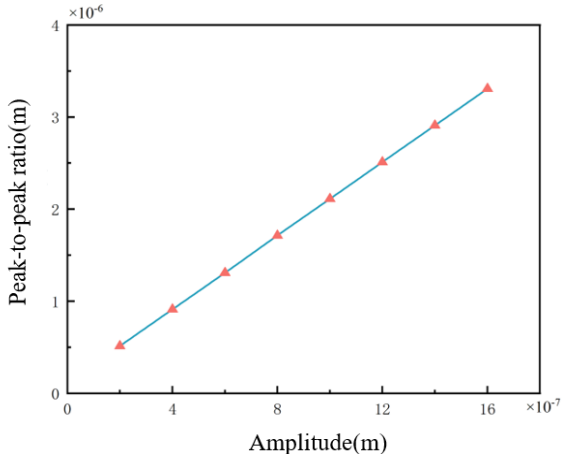

Figure 13 The effect of the waviness amplitude of the outer ring on the peak-to-peak value of the vibration displacement in the y-axis direction of the bearing

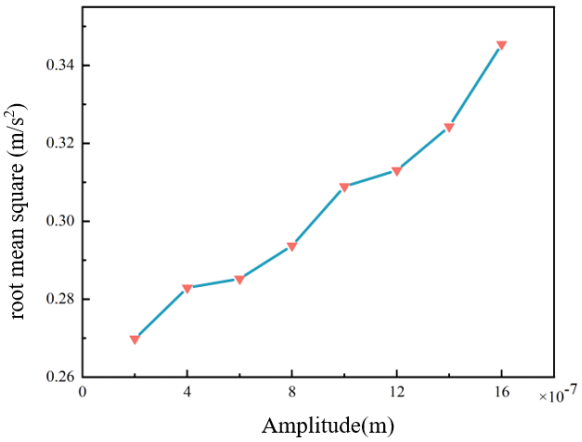

Figure 14 The influence of the waviness amplitude of the outer ring on the RMS value of vibration acceleration in the y-axis direction of the bearing

5 Conclusion

Different from previous studies, this work focuses on exploring the key scientific problems of deep groove ball bearing damage dynamic mechanism mining and the key technical problems of deep groove ball bearing dynamic optimization control that urgently need to be solved in the RV reducer production industry. Taking 6308 deep groove ball bearing as the research entry point, a sinusoidal based raceway surface waviness model is established. The dynamic model of 2-degree-of-freedom deep groove ball bearing was improved, and the numerical solution of the characteristic dynamic parameters of the model was obtained by using the fourth-order Runge-Kutta algorithm. The relevant findings are summarized below:

(1) As the waviness amplitude of the raceway surface and outer ring increases, the vibration displacement of the bearing inner ring in the y-axis direction and the peak-to-peak value of vibration displacement increase, that is, the bearing vibration amplitude increases with the increase of the waviness amplitude of raceway surface.

(2) The vibration acceleration value of the bearing inner ring in the y-axis direction increases with the increase of waviness amplitude of the raceway surface and outer ring surface, that is, the energy of impact waveform induced by waviness increases with the increase of waviness amplitude of raceway surface.

Finally, the development of this research work contributes to digging deeper into the precision bearing processing raceway surface accuracy induced by the heterogeneous irregular waviness on the bearing vibration characteristics of the influence of the law, helps to explore the harsh operating conditions of the bearing running state real-time health monitoring to provide a certain degree of scientific reference and engineering reference.

References

[1] Yu G, Su M, Xia W, et al. Vibration characteristics of deep groove ball bearing based on 4-DOF Mathematical Model[J]. Procedia Engineering, 2017(174):808-814.

[2] Zhi-Jie J, Bin Z, You-Liang Z, et al. Analysis of the miniature deep groove ball bearing radial clearance loaded measuring method[J]. Journal of Mechanical & Electrical Engineering, 2015,32(2):223-227.

[3] Kankar P K, Sharma S C, Harsha S P. Nonlinear vibration signature analysis of a high speed rotor bearing system due to race imperfection[J]. Journal of Computational and Nonlinear Dynamics, 2012 (1):11014.

[4] Shah D S, Patel V N. Theoretical and experimental vibration studies of lubricated deep groove ball bearings having surface waviness on its races[J]. Measurement, 2018(129):405-423.

[5] Sun M, Xu H, An Q. Noise calculation method of deep groove ball bearing caused by vibration of rolling elements considering raceway waviness[J]. Proceedings of the Institution of Mechanical Engineers, Part C: Journal of Mechanical Engineering Science, 2021,236(8):4429-4439.

[6] Yang M, Lu H, Zhang X, et al. Influence of surface waviness of journal and bearing bush on the static characteristics of hydrodynamic bearing[J]. Processes, 2021, 9(1):110.

[7] Jing L, Ruikun P, Yajun X U, et al. Vibration analysis of a single row angular contact ball bearing with the coupling errors including the surface roundness and waviness[J]. Science China: Technological Sciences, English Edition, 2020,63(6):10.

[8] Tallian T E, Gustafsson O G. Progress in rolling bearing vibration research and control[J]. A S L E Transactions, 1965,8(3):195-207.

[9] Choudhury A, Tandon N. A theoretical model to predict vibration response of rolling bearings to distributed defects under radial load[J]. Journal of vibration and acoustics: Transactions of the ASME, 1998 (1):120.

[10] Aktu Rk N. The effect of waviness on vibrations associated with ball bearings[J]. Journal of Tribology, 1999(9):45-48.

[11] Li H, Du G. Characterization of radial stiffness of high-speed deep groove ball bearings considering elastic flow lubrication[J]. Bearing, 2021(10):10-13+19.

[12] Yong C, Li X. Research on the conversion method of effective value between vibration acceleration, velocity and displacement[J]. Light Industry Science and Technology, 2024,40(1):70-72.

Viser Technology Pte. Ltd.
Mechanical Engineering Science
DOI: 10.33142/mes.v6i1.13224

Research Article Open Access

An Improved Harris Hawk Optimization Algorithm

GuangYa Chong, Yongliang YUAN*

He'nan Polytechnic University, Jiaozuo, He'nan, 454150, China

***Corresponding Author:** *Yongliang YUAN, E-mail: yuanyongliang@hpu.edu.cn*

Abstract

Aiming at the problems that the original Harris Hawk optimization algorithm is easy to fall into local optimum and slow in finding the optimum, this paper proposes an improved Harris Hawk optimization algorithm (GHHO). Firstly, we used a Gaussian chaotic mapping strategy to initialize the positions of individuals in the population, which enriches the initial individual species characteristics. Secondly, by optimizing the energy parameter and introducing the cosine strategy, the algorithm's ability to jump out of the local optimum is enhanced, which improves the performance of the algorithm. Finally, comparison experiments with other intelligent algorithms were conducted on 13 classical test function sets. The results show that GHHO has better performance in all aspects compared to other optimization algorithms. The improved algorithm is more suitable for generalization to real optimization problems.

Keywords: *Harris Hawk optimization algorithm; chaotic mapping; cosine strategy; function optimization*

1 Introduction

With the advancement of technology and the complexity of problems, optimization tasks often exhibit characteristics such as multi-objective, large-scale, uncertainty, and complexity, which are difficult to resolve [1]. In the real world, most problems have multiple constraints and optimization objectives, while traditional optimization algorithms [2-3] mainly focus on a single objective, which makes it difficult to solve real-world problems [4-7]. It is due to these shortcomings of traditional optimization algorithms that metaheuristic optimization algorithms have emerged, which are better able to solve complex engineering problems [8]. Metaheuristic algorithms are mostly inspired by natural phenomena and are considered as the best optimization algorithms globally due to their superior performance. With the continuous exploration of optimization algorithms, many metaheuristic algorithms have been generated, such as Dragonfly Algorithm [9], Snake Optimizer [10], White Shark Optimize [11], Sine cosine algorithm [12], Atomic Orbital Search [13], etc. Harris Hawk optimization algorithm is a metaheuristic optimization algorithm proposed by Haidari et al. in 2019. [14]. The algorithm can utilize simpler and practical processing methods to simplify the problem and has relatively good performance. However, the Harris Hawk optimization algorithm suffers from low precision of the results and low values of convergence speed. Therefore, to solve these problems, we improved the algorithm and named it GHHO. Firstly, population initialization is a crucial step in the optimization algorithm, which plays a vital role in both the performance and convergence speed of the algorithm. The Gauss mapping method is used to obtain the initial HHO population, which solves the problem of non-uniform distribution of initial positions in the search space, and makes the population distribution more uniform and diverse. Secondly, the computational accuracy of the algorithm is improved by changing the original parameters through Gauss chaotic mapping. Finally, a cosine strategy is introduced into the algorithm, which prevents the algorithm from falling into a local optimum.

2 Harris Hawks Optimization (HHO)

The Harris' hawk is found mainly in the United States and is a fierce bird. They will cooperate with each other in the hunting process, and increase the success rate through coordinated hunting. During the hunting process, Harris's hawks often use "raids", where they attack through multiple individuals and multiple angles of encirclement. This "raiding" behavior highlights the foraging characteristics of this species, and makes it difficult for prey to escape from encirclement due to the rapidity and frequency of their attacks. This species also changes its hunting mode according to the escape characteristics of the prey, so that the hunting process can be adapted to the situation and the prey can be obtained efficiently. Heidari et al. fully studied the hunting behavior of Harris's hawk and constructed the mathematical model of HHO by combining with Gray

Received on May 8, 2024; Accepted on May 29, 2024

Wolf Optimization (GWO) algorithm. We assume the behavior of Harris Hawk in acquiring prey as two phases: exploration and exploitation. The amount of escape energy E will determine whether the algorithm is in the exploratory or exploitation stage; when in the exploitation stage, the attack strategy can be categorized into soft and hard besiege according to the escape energy when the random number r is not less than 0.5. On the contrary, when r is less than 0.5, it can also be categorized into soft besiege with progressive rapid dives and hard besiege with progressive rapid dives based on the escape energy.

2.1 Exploration phase

When $|E| \geq 1$, GHHO is in an exploratory phase. The location update can be categorized into two strategies based on the Harris's hawk's perching situation q, as shown in Eq (1-2):

$$X(t+1) = X_{rand}(t) - r_1 \left| X_{rand}(t) - 2r_2 X(t) \right| \quad q \geq 0.5 \tag{1}$$

$$X(t+1) = (X_{rabbit}(t) - X_m(t)) - r_3(LB + r_4(UB - LB)) \quad q < 0.5 \tag{2}$$

Where $X(t+1)$ is the coordinates of the Harris' hawk at t+1 iteration; $X_{rand}(t)$ is the coordinates of the species in the randomized case at the tth iteration; $X_{rabbit}(t)$, $X_m(t)$ are the prey-specific coordinates at the tth iteration, and the coordinates of the midpoint of the Harris' hawk; LB, UB are numerical range thresholds; r_1 , r_2 , r_3 *and* r_4 are random numbers inside (0,1).

During the iteration process, the escape energy E decreases gradually as shown in Eq (3):

$$E = 2E_0\left(1 - \frac{t}{T}\right) \tag{3}$$

Where T , t and E_0 represent the maximum number of iterations, the current number of iterations and the initial energy value of E, respectively.

2.2 Exploitation phase

When $|E| < 1$, hunting can be further categorized into four different strategies.

a. Soft besiege

When $r \geqslant 0.5$ and $|E| \geq 0.5$, the algorithm implements this strategy as shown in Eq (4), with J being the escape of the besieged species. r_5 is a random number between 0 and 1

$$X(t+1) = X_{rabbit}(t) - X(t) - E\left| JX_{rabbit}(t) - X(t) \right| \tag{4}$$

$$J = 2(1 - r_5) \tag{5}$$

b. Hard besiege

When $r \geq 0.5$ and $|E| < 0.5$, Harris' hawk adopts a hard besiege, see Eq (6). At this point, the Harris's hawk will be a one-strike winner as the prey has been escaping resulting in a decrease in escape level.

$$X(t+1) = X_{rabbit}(t) - E\left| X_{rabbit}(t) - X(t) \right| \tag{6}$$

c. Soft besiege with progressive rapid dives

When still $|E| \geq 0.5$ but $r < 0.5$, since the prey has enough stamina to escape, the Harris' hawk will start a high-speed dive, which is still a soft besiege. If the raid is unsuccessful, it will turn on random wandering Z , and if the wandering is unsuccessful it will return to the initial position, the strategy is shown in equation (7-8):

$$Y = X_{rabbit}(t) - E\left| JX_{rabbit}(t) - X(t) \right| \tag{7}$$

$$Z = Y + S \times LF(D) \tag{8}$$

Where S and D represent the random number and dimension, respectively. LF is the levy flight function, as shown in Eq (9):

$$LF(x) = 0.01 \times \frac{u \times \sigma}{|v|^{\frac{1}{\beta}}}, \sigma = \left(\frac{\Gamma(1+\beta) \times sin(\frac{\pi\beta}{2})}{\Gamma(\frac{1+\beta}{2}) \times \beta \times 2^{(\frac{\beta-1}{2})}} \right)^{\frac{1}{\beta}} \tag{9}$$

Where, u, v are random numbers in the range of (0,1) and the value of β is 1.5.

d. Hard besiege with progressive rapid dives

When $|E| < 0.5$ and $r < 0.5$, the Harris' hawk based on the location of the center of the group in relation to where the prey is located, with reference to Eq (10) for the specific strategy.

$$Y = X_{rabbit}(t) - E\left| JX_{rabbit}(t) - X_m(t) \right| \tag{10}$$

3 Improved Harris Hawk Optimization (GHHO)

3.1 Initialization of Gauss chaos mapping

HHO is randomly generated by the computer, which tends to make the individual fitness of the initial population deviate from the optimal fitness, thus making the algorithm converge slowly and generating high running time, leading to the degradation of the solution quality. The author adopts Gauss chaotic mapping to initialize the population and ensure the diversity of the population. As shown in Eq (11):

$$x_{n+1} = f(x_n) = \begin{cases} 1 & x_n = 0 \\ \dfrac{1}{\mathrm{mod}(x_n, 1)} & \text{otherwise} \end{cases} \tag{11}$$

3.2 Optimization of energy parameters

In response to the suspension of the HHO due to early convergence, the author uses Gauss chaotic mapping to optimize the energy parameter E. Finally, it is shown that this method can improve the function difficulties and improve the accuracy and robustness. The improvement is shown in Eq (11):

$$E = 2E_0\left(1 - \frac{t}{T}\right) \times f(x_n) \tag{12}$$

3.3 Cosine strategy

In order to solve the problem of low accuracy of results and easy to fall into local optimum in the use of HHO method, the author introduced the cosine strategy in Eq (2), which improves the performance of the optimization algorithm solution. As shown in Eq (13):

$$X(t+1)=(X_{rabbit}(t)-X_m(t))-r_3(LB+r_4(UB-LB))\times\cos(r_5+1) \quad q<0.5 \tag{13}$$

Where, r_5 is a random number lies in the range of (0, 1).

3.4 Algorithm flow chart

Combining the above improvement strategies, the GHHO algorithm flow is shown in Figure 1.

Step 1: Gauss population initialization, set population size N, dimension D, initialize each parameter.

Step 2: Gauss optimizes the energy parameter E. The optimized E is applied to Eqs. (4), (6), (7) and (10) to update the population position.

Step 3: Introduce the cosine strategy into Eq. (2) in the exploratory phase, a phase in which the population will use Eq. (13) to update its position.

Step 4: Determine whether the termination condition is reached, if so, output the optimal value; otherwise, return to step 2.

The GHHO algorithm records the position of the population from the first iteration and each iteration is compared with the results of the last iteration until the last iteration is completed. The best candidate solution saved during the iterations is used as the final solution to the problem after the algorithm is completely finished.

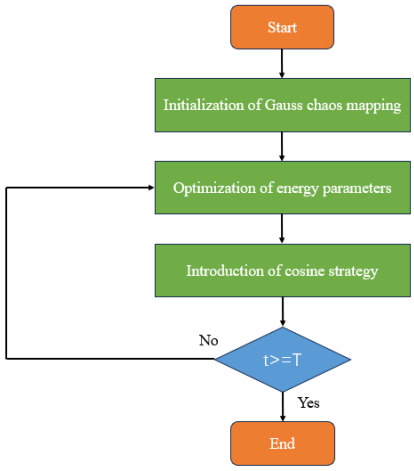

Figure 1 Flow chart of GHHO

Table 1 Statistical results of test functions

Function		GWO	BOA	MFO	GA	PSO	GHHO
F1	Avg	3.64E-174	1.93E-17	1.79E+03	1.63E-02	7.55E-04	0.00E+00
	Std	0.00E+00	9.38E-19	3.87E+03	4.59E-03	7.06E-04	0.00E+00
F2	Avg	1.22E-99	1.51E-14	2.96E+01	3.19E-01	1.43E-02	2.64E-270
	Std	2.84E-99	1.74E-15	2.20E+01	4.70E-02	7.87E-03	0.00E+00
F3	Avg	1.97E-55	2.02E-17	1.36E+04	2.44E+02	1.80E+01	0.00E+00
	Std	1.35E-54	9.95E-19	1.20E+04	4.89E+02	4.89E+00	0.00E+00
F4	Avg	8.73E-44	1.64E-14	1.42E+01	1.57E-01	8.77E-01	1.17E-268
	Std	4.17E-43	7.52E-16	8.62E+00	1.89E-02	1.48E-01	0.00E+00
F5	Avg	2.59E+01	2.90E+01	3.11E+04	3.40E+01	9.60E+01	2.32E-02
	Std	8.57E-01	2.59E-02	4.79E+04	2.11E+01	7.34E+01	2.44E-02
F6	Avg	1.28E-01	4.86E+00	2.10E+03	7.85E+00	6.80E-04	2.07E-05
	Std	1.91E-01	5.84E-01	3.43E+03	1.01E-01	7.38E-04	3.55E-05
F7	Avg	1.23E-04	2.26E-04	1.68E+00	8.56E-01	1.93E-01	1.84E-05
	Std	7.87E-05	8.01E-05	4.30E+00	2.29E-01	8.26E-02	5.46E-06
F8	Avg	-6.45E+03	-4.78E+03	-9.00E+03	-2.66E+03	-6.81E+03	-1.07E+04
	Std	6.60E+02	3.65E+02	8.50E+02	5.04E+02	8.56E+02	1.93E+03
F9	Avg	0.00E+00	1.89E+00	1.18E+02	1.82E+00	4.86E+01	0.00E+00
	Std	0.00E+00	1.89E+01	3.82E+01	5.46E-01	1.35E+01	0.00E+00
F10	Avg	8.03E-15	1.04E-14	8.03E-15	8.41E-02	1.81E-02	4.44E-16
	Std	9.44E-16	3.60E-15	9.44E-16	1.60E-02	1.10E-02	0.00E+00
F11	Avg	4.52E-04	0.00E+00	4.52E-04	5.91E-04	1.39E-02	0.00E+00
	Std	2.30E-03	0.00E+00	3.30E-03	2.75E-04	1.21E-02	0.00E+00
F12	Avg	1.28E-02	2.86E-01	2.28E-02	2.69E+00	4.08E-06	6.25E-07
	Std	9.31E-03	8.30E-02	9.31E-03	4.39E-02	4.43E-06	8.09E-07
F13	Avg	1.55E-01	1.69E+00	2.55E-01	2.93E-03	9.67E-04	7.70E-05
	Std	1.25E-01	4.39E-01	3.24E-01	7.13E-04	2.62E-03	1.46E-04

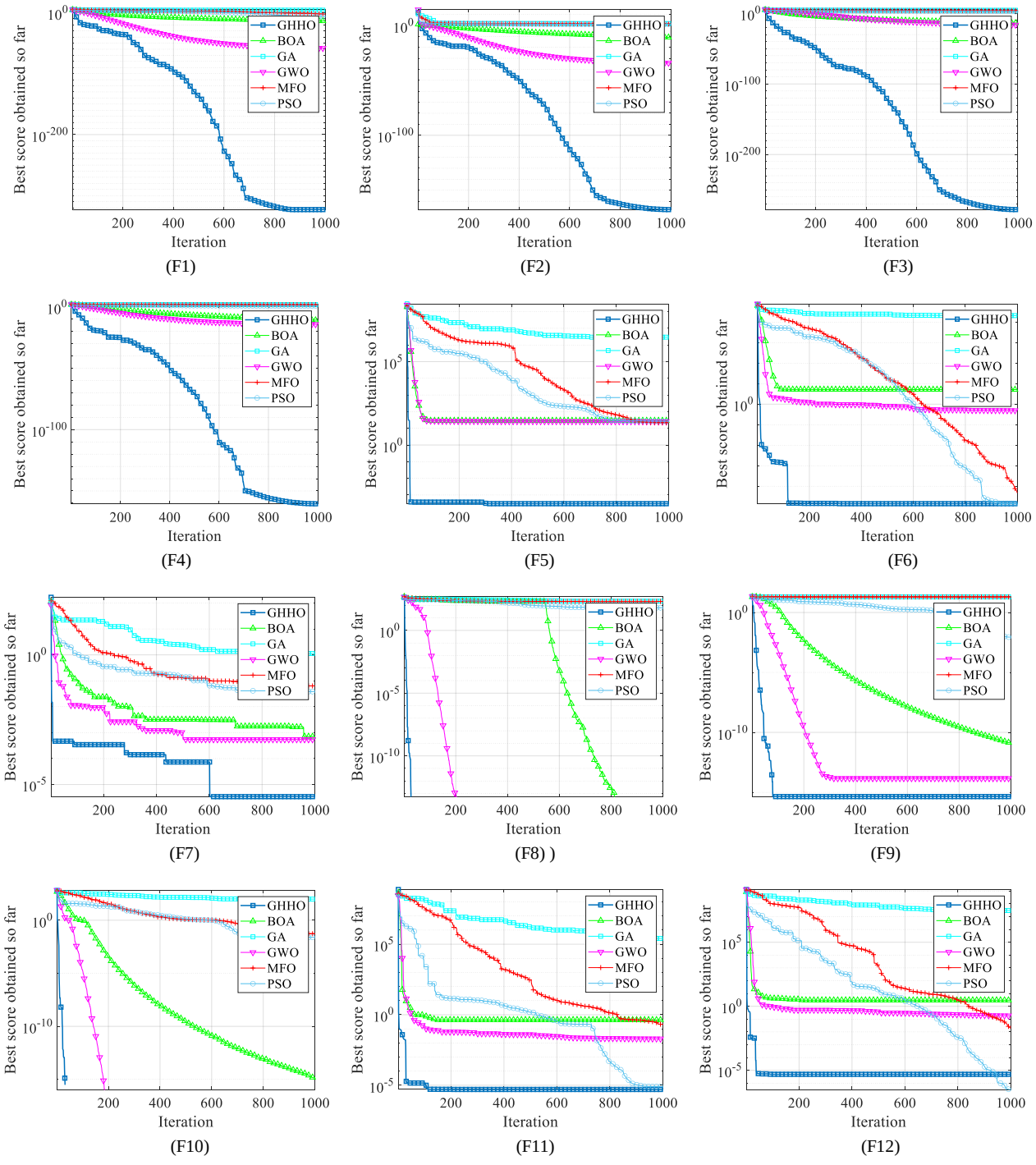

Figure 2 Convergence Curve

4 Experimental Design

This experiment is designed to examine the performance of each algorithm with 13 typical global optimization test functions from the literature [15]. These classical functions are categorized into single-peak and multi-peak functions.

We compare GHHO with GWO [16], BOA[17], MFO[18], GA[19] and PSO [20]respectively. During the experiments, the population size and dimension of each algorithm is set to 30 and the maximum number of iterations is set to 1000.

Table 1 presents the competitive results of the GHHO algorithm on F1-F13. It is clear that GHHO performs well in terms of overall performance, specifically, GHHO obtains the best solution for all tested functions except F8. Figure 2 demonstrates the convergence process of all algorithms except F8, and GHHO exhibits higher convergence accuracy compared to other optimization algorithms, which also validates the experimental data in Table 1.

These results show the excellent performance of the GHHO algorithm in dealing with single-peak benchmark functions (F1-F7) and multi-peak functions (F8-F13), which further validates the accuracy and reliability of the GHHO algorithm as well as its excellent performance on different types of optimization problems.

5 Conclusion

In this work, an optimization algorithm GHHO with better performance is proposed based on HHO. Firstly, Gaussian chaotic mapping strategy is used to initialize the population. Secondly, by optimizing the energy parameters and introducing the cosine strategy, GHHO possesses a better performance. Finally, the effectiveness of GHHO is verified by comparing it with different intelligent optimization algorithms on test functions.

References

[1] Wan M, Ye C, Peng D. Multi-period dynamic multi-objective emergency material distribution model under uncertain demand[J]. Eng Appl Artif Intell, 2023(117):105530.

[2] Inceyol Y, Cay T. Comparison of traditional method and genetic algorithm optimization in the land reallocation stage of land consolidation[J]. Land Use Policy, 2022(115):105989.

[3] Wang W-c, Xu L, Chau K-w, et al. An orthogonal opposition-based-learning Yin–Yang-pair optimization algorithm for engineering optimization[J]. Eng Comput, 2022(38):1149–1183.

[4] Atban F, Ekinci E, Garip Z. Traditional machine learning algorithms for breast cancer image classifcation with optimized deep features[J]. Biomed Signal Process Control, 2023(81):104534.

[5] Hu G, Chen L, Wei G. Enhanced golden jackal optimizer-based shape optimization of complex CSGC-Ball surfaces[J]. Artif Intell Rev, 2023(56):2407–2475.

[6] Wang L, Gao K, Lin Z, et al. Problem feature based meta-heuristics with Q-learning for solving urban trafc light scheduling problems[J]. Appl Soft Comput, 2023(147):110714.

[7] Wang W-c, Xu L, Chau K-w, et al. Cε-LDE: a lightweight variant of differential evolution algorithm with combined ε constrained method and Lévy fight for constrained optimization problems[J]. Expert Syst Appl, 2023(211):118644.

[8] Ayyarao T S L V, Ramakrishna N S S, Elavarasan R M, et al. War strategy optimization algorithm: a new effective metaheuristic algorithm for global optimization[J]. IEEE Access, 2022(10):25073-25105.

[9] Mirjalili S. Dragonfly algorithm: a new meta-heuristic optimization technique for solving single-objective, discrete, and multi-objective problems[J]. Neural computing and applications, 2016(27):1053-1073.

[10] Hashim F A, Hussien A G. Snake Optimizer: A novel meta-heuristic optimization algorithm[J]. Knowledge-Based Systems, 2022(242):108320.

[11] Braik M, Hammouri A, Atwan J, et al. White Shark Optimizer: A novel bio-inspired meta-heuristic algorithm for global optimization problems[J]. Knowledge-Based Systems, 2022(243):108457.

[12] Mirjalili S. SCA: a sine cosine algorithm for solving optimization problems[J]. Knowledge-based systems, 2016(96):120-133.

[13] Azizi M. Atomic orbital search: A novel metaheuristic algorithm[J]. Applied Mathematical Modelling, 2021(93):657-683.

[14] HEIDARI A A, MIRJALILI S, FARIS H, et al. Harris hawks optimization: Algorithm and applications[J]. Future generations computer systems (FGCS), 2019(97):849-872.

[15] YAO Xin, LIU Yong, LIN Guangming. Evolutionary programming made faster[J]. IEEE transactions on evolutionary computation, 1999,3(2):82-102.

[16] Mirjalili S, Mirjalili S M, Lewis A. Grey wolf optimizer[J]. Advances in engineering software, 2014(69):46-61.

[17] Arora S, Singh S. Butterfly optimization algorithm: a novel approach for global optimization[J]. Soft computing, 2019(23):715-734.

[18] Mirjalili S. Moth-flame optimization algorithm: A novel nature-inspired heuristic paradigm[J]. Knowledge-based systems, 2015(89):228-249.

[19] Deb K. Optimal design of a welded beam via genetic algorithms[J]. AIAA journal, 1991,29(11):2013-2015.

[20] Wang D, Tan D, Liu L. Particle swarm optimization algorithm: an overview[J]. Soft computing, 2018,22(2):387-408..

Viser Technology Pte. Ltd.
Mechanical Engineering Science
DOI: 10.33142/mes.v6i1.13225

Research Article Open Access

Research on the Application of Intelligent Optimization Algorithm in Mechanical Design

Donglai LUAN

University of Shanghai for Science and Technology, Shanghai, 200093, China

*Corresponding Author: Donglai LUAN, E-mail: ldl150126@163.com

Abstract

Intelligent optimization algorithm belongs to a kind of emerging technology, show good characteristics, such as high performance, applicability, its algorithm includes many contents, including genetic, particle swarm and artificial neural network algorithm, compared with the traditional optimization way, these algorithms can be applied to a variety of situations, meet the demand of solution, in the mechanical design industry has wide application prospects. This paper analyzes the application of the algorithm in mechanical design and the comparison of the results to verify the significance of the intelligent optimization algorithm in mechanical design.

Keywords: intelligent optimization algorithm; mechanical design; application

1 Introduction

With the development of science and technology, the mechanical design is more complex, and the design difficulty is gradually increasing, and the traditional algorithm cannot meet the needs of mechanical design. Most of the traditional algorithms rely on manual design, which requires high time and cost. Through the application of intelligent optimization algorithm, related problems can be effectively solved. Intelligent optimization algorithm refers to the intelligent phenomenon displayed by the natural biological groups as the basis of the design activities, which can carry out self-evolution and adaptation.

2 The Application Significance of Intelligent Optimization Algorithm in Mechanical Design

Based on the development of social economy and the emergence of the trend of informatization, computer technology has played an important role in the processing of engineering problems. In recent years, the development of science and technology is characterized by the coordinated development of biology and engineering technology, which permeates each other and promotes the improvement of the teaching effect. Scholars and experts have created new algorithms, namely intelligent optimization algorithms, for the simulation of life science in studying natural phenomena. The algorithm involves many disciplines and belongs to the multi-disciplinary computational science, which has attracted the attention of experts and scholars. Due to its high efficiency and applicability, its application to mechanical design can provide new ideas for the solution of complex engineering problems and contribute to the effective solution of problems. At the same time, the algorithm has the advantages of versatility and robustness, in computer, engineering optimization and other fields, showing a good application prospect.

First, intelligent optimization algorithm contains many contents, such as simulating genetics, particle swarm and artificial neural network and annealing method of metal cooling. Compared with the traditional optimization method, the optimization method is highly adaptable, which can meet the design solution requirements under various links, and contribute to the improvement of design results.

Secondly, in the design link of engineering products, the intelligent optimization algorithm plays an important role, and it has been widely used since its inception. Through the development of the optimized design, the product can have good parameters, achieve the best quality size results, truly achieve the relevant goals, and reduce the investment. In the current environment, intelligent optimization algorithm has been applied in various industries, including national defense, construction, industrial machinery and petrochemical industry, etc., contributing to various industries and showing a vigorous development trend.

Finally, the optimized design has been widely used in mechanical design. Through the integration of this concept, it is conducive to the design of good mechanical

Received on May 3, 2024; Accepted on May 30, 2024

products, meet the requirements of various properties, and achieve better results. In the mechanical design activities, with the help of computer assistance, we can shorten the practice of scheme selection, select the optimal scheme in the shortest time, and promote the significant improvement of design efficiency. In the process of mechanical optimization design, tend to design to the mathematical theory content, prone to local optimal value and the target function has higher requirements, and the traditional optimization way, cannot meet the requirements of the design of various conditions, with the help of intelligent optimization theory, can solve the problems of traditional optimization, good mechanical design effect.

3 The Theoretical Basis of the Intelligent Optimization Algorithm

Intelligent optimization algorithm is based on the nature, research activities, the character content, in the simulation of natural phenomena and laws, gradually derived a variety of bionic algorithms. In addition, in the intelligent optimization algorithm, mathematical theory belongs to the basis, can adopt computer technology, the solution of a group of problems set as the initial, according to the solution parameters of the problem, according to the relevant provisions, to carry out operational activities. Different from the traditional optimization algorithm, the intelligent optimization algorithm belongs to the probability search method, which has obvious advantages: the algorithm can be optimized according to the value of the objective function to escape the influence of the differentiability of the objective function; the algorithm is not affected by the central constraint and will not affect the overall problem due to individual operators, which can guarantee the system robustness; it has a broad applicable scope and can carry out large-scale operation. In the intelligent optimization algorithm, genetic, particle swarm and annealing algorithms have been widely used. The main algorithm studied in this paper is genetic and particle swarm algorithm, which provides guarantee for the subsequent research by analyzing its characteristics.

3.1 Genetic algorithm

American Holland first proposed the genetic algorithm in 1975, and the algorithm mainly comes from the research of biological systems, using the computer simulation in the process of research. Genetic algorithm is mainly through the biological evolution, genetics, the formation of technology model, with the simulation of natural evolution process, form the best quality solution, belongs to the efficient search way, can guarantee the global search, the way can be through the way of automatic search, analysis of spatial information, and get the optimal solution. Genetic algorithm mainly follow the related principles of nature, namely the principle of survival of the fittest, by coding the characters and code for chromosome, and the composition of each population for N individuals, and individual formed by string structure, the individual become the research object of genetic algorithm, can carry out efficient search activities in the parameter space, operating random optimization.

In addition, genetic algorithms do not need the help of auxiliary information. The algorithm has a good fitness function, which breaks the limit of continuity and differentiability, and can evaluate the optimal unit with the help of the fitness function. At the same time, at the same time, it can set a wide range of value categories, break the constraints of the operation, and promote the expansion of the application scope.

3.2 Particle swarm algorithm

American James Kennedy and Russell Eberhart formally proposed the concept of particle swarm algorithm in 1995. The algorithm is mainly based on the predation of birds, and it belongs to a random search method based on group collaboration, and shows a good application prospect. Particle swarm algorithm is to find the best solution by using the cooperative activities of groups and individuals, so as to find the optimal solution.

4 Application of Intelligent Optimization Algorithm in Mechanical Design

4.1 The application of the intelligent optimization algorithm in the traction machine

In the process of elevator operation, the traction machine plays an important role, belongs to the mechanical transmission facilities, there are widely used, in the current era, the traction machine has some shortcomings, such as large volume, large transmission ratio, resulting in the actual mechanical efficiency is poor. Therefore, in order to improve the mechanical efficiency and reduce the power consumption, in the research field of traction machine, the light quality, high efficiency and strong bearing capacity have become the main direction. However, in addition to optimizing the materials and processing methods of tractors, it is also necessary to pay attention to the adjustment of optimization methods, optimize the design of tractors, and ensure the good development of tractors.

For example, the tractor adopted by an elevator is selected as a case, and according to the ordinary cylindrical worm reducer, including input power (P 1 5.5 Kw), rotation speed (n11400 r/min), load coefficient (K 1.1) and transmission ratio (i 20). In addition, the worm material is selected as low carbon alloy steel, the turbine material is cast tin bronze, and the allowable stress of the turbine gear ring in the tractor is 220MPa. In the optimization, it is necessary to clear the optimization goal, meet the strength, stability and stiffness of all

parties as the basis, pay attention to the adjustment of mechanical design, so as to realize the reduction of the turbine tooth ring, reduce the material input, and improve the work efficiency of the traction machine.

Through the arrangement of target and constraint functions, the algorithm program can be written, including particle swarm algorithm and legacy particle swarm algorithm. Multiple programming and debugging activities can obtain stable results and ensure normal output. The specific results are shown in Figure 1 and Figure 2.

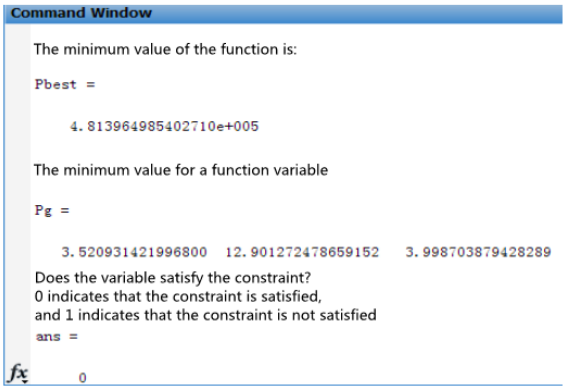

Figure 1 Pswarm algorithm results

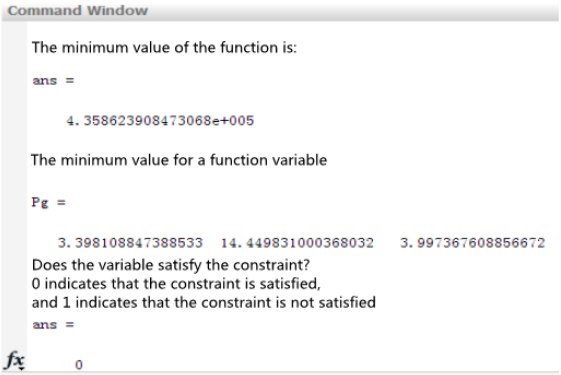

Figure 2 Heritage particle ensemble combined with the algorithm results

Take the way of comparison, you can select the best optimization effect of the algorithm. By comparing the results of traditional optimization, particle swarm and genetic particle swarm combined with algorithms (such as Table 1), it is not difficult to draw the following conclusions: the conclusion of intelligent optimization algorithm is obviously better than the results of traditional optimization methods. Compared with the traditional optimization way, the particle swarm results are roughly lower than the traditional algorithm 27 percent, genetic particle swarm combining the results of roughly lower than the traditional algorithm, according to the table of the data analysis, can find the intelligent optimization algorithm applied to the design link, can effectively optimize the turbine volume, although the genetic and particle group algorithm has good optimization results, but the best optimization algorithm is genetic particle swarm algorithm, the application of mechanical design link, can significantly improve the design effect.

4.2 Application of intelligent optimization algorithm in spring

In the mechanical industry spring has a very wide application, belongs to the important connection part of mechanical equipment, instruments and other items, belongs to a kind of elastic elements. Spring has a unique elastic function, can accept load after elastic deformation, when eliminate load, the spring can return to the original state, in the process of spring deformation, realize the mechanical energy, elastic potential energy and kinetic energy conversion, at the same time because of its characteristics, meet the demand of all kinds of machinery. In the process of spring optimization design, the key contents are the number of spring coil, spring wire and medium diameter. Through the optimization design activities of the above parameters, the design objectives are clear, the focus is on reducing the weight of the spring, and the cost reduction is realized.

For example, you can select a spring to apply to an elevator speed limiter as a case to identify all kinds of data of the spring, including diameter (44mm) and maximum stiffness (K_{max}24 N/mm), allowable stress (665 Mpa) and the maximum working pressure (F_{max}1120N) .At the same time, when optimizing the design of the spring, it is necessary to identify the best spring working ring (n), spring diameter (d) and spring diameter (D) from the required perspective.

By sorting out the target and constraint functions, and writing relevant programs, including particle swarm algorithm and genetic particle group combination, programming and debugging activities, the stability of the output operation results is finally guaranteed. The specific results are shown in Figure 3 and Figure 4.

Table 1 Comparison of the algorithm results

optimization method	Number of worm heads, z_1	modulus m mm	Diametral quotient q	volume V mm^3
Traditional optimization method	3	5	8	692436.2344
particle swarm optimization	4	3.5	14	507635.8750
Genetic particle swarm combination algorithm	4	3.5	13	475908.6330

Table 2 Comparison of the algorithm results

Optimization method	Number of effective coils n	The reed diameter d mm	In the spring through d mm	Volume v mm^3
Traditional optimization method	15	6	36	47963.4481
Particle swarm optimization	27	5	22	36638.7451
Genetic particle swarm combination algorithm	23	5	23	32629.4548

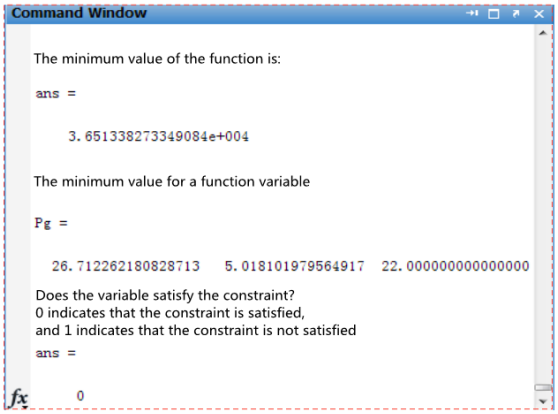

Figure 3 Pswarm algorithm results

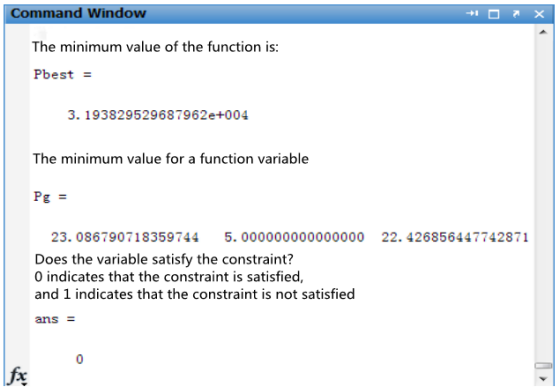

Figure 4 Combined algorithm results of legacy particle groups

Through the algorithm comparison, the final solution results are obtained, including traditional optimization, the combination of genetic particle groups and particle group. The specific display is shown in Table 2. Through the development of relevant data analysis, it is not difficult to find the application of intelligent optimization algorithm, and the results are significantly better than the traditional methods. By carrying out comparative activities with the traditional way, it can be concluded that compared with the traditional algorithm, the particle group is reduced by nearly 24%, and the combination of genetic particle group is reduced by nearly 32% compared with the traditional algorithm. According to the above results, it can be found that the intelligent optimization algorithm can achieve good results in the application process of spring volume optimization. Although the genetic and particle swarm algorithm have good optimization results, the most obvious effect is still the genetic particle swarm combination algorithm proposed in this paper.

5 Conclusion

To sum up, under the background of the information age, the machinery industry has ushered in the opportunities and challenges of development. In order to better seize the opportunities and meet the challenges, it is necessary to pay attention to the optimization of mechanical design and change the previous algorithm form. This paper discusses the application effect of intelligent optimization algorithm, and takes the traction machine and spring as cases. Compared with previous optimization algorithms, intelligent optimization algorithm has outstanding advantages in search, design and other aspects. The application of this algorithm in mechanical design is helpful to optimize the design effect. Among them, the intelligent optimization algorithm has more prominent advantages, which can be better optimized and achieve good results. A new genetic particle swarm combination algorithm is proposed to achieve outstanding results in mechanical design.

References

[1] Fang Chen cheng, Pan Die, Zhang Fengfei. Design of ultra-thin mechanical structure of four-way vehicles and optimization of intelligent control algorithm[J]. Modern Manufacturing Technology and Equipment, 2024,60(2):114-117.

[2] Zhou Dongdong, Liu Yuhui, He Yuhan. Energy-saving optimization design of mechanical equipment in smart city based on intelligent algorithm[C]. Proceedings of the 4th Electric Power Engineering and Technology Academic Exchange Conference, 2023.

[3] Xu Xiangyi, Zhao Zhengying. Application of group intelligence algorithm in Optimization Design of Fuzzy Controller[J]. Computer Programming Skills and Maintenance, 2021(9):136-137 + 159.

[4] Chen Baofa, Hong Fangchi, Xu Xu. Application of intelligent algorithm in the optimal design of steam pipe network [J]. Journal of China University of Metrology, 2021,32(2):203-209.

[5] Zhao Zhuanzhe, Liu Yongming, Zhang Zhen, et al. Application of group intelligent algorithm in the teaching of "Mechanical Optimization Design"[J]. Journal of Wuzhou University, 2021,31(3):67-74.

Viser Technology Pte. Ltd.
Mechanical Engineering Science
DOI: 10.33142/mes.v6i1.13226

Research Article Open Access

Design and Numerical Simulation of Dust Removal System for Sutomotive Iongitudinal Beam Plasma Cutting

Wenqiang GAO, Xudong MA*, Heyu TIAN

Changchun Technical University of Automobile, Changchun, Jilin, 130013, China

*Corresponding Author: Xudong MA, E-mail: 279667122@qq.com

Abstract

To improve the poor efficiency of the dust removal system in the plasma cutting station of automotive longitudinal beams, and reduce the cutting surface quality degradation due to dust, a bottom-side suction dust removal system is designed, and the dust removal effect is optimized through the setting of the following dampers and diversion plates. The result of numerical simulation indicates that the particle collection rate can reach 99.44%, and the field test also proves the effectiveness of the dust removal system, which is of guiding significance for the transformation of other similar dust removal systems.

Keywords: *plasma cutting; dust removal equipment; simulation*

1 Introduction

Plasma cutting is a commonly used cutting method, the main principle of which is to heat the machine part through a high-temperature plasma arc, so that the material locally melts under the high temperatures, evaporates or goes out with the high speed plasma, and finally forms the processing method of cutting [1]. Because of the high cutting speed, high efficiency, good cutting surface, accurate size and flexibility with various working gases, plasma cutting is widely used in aerospace, machining, electrical and electronic areas, and can be use for cutting aluminum, copper, titanium, galvanized steel and other materials which are difficult to cut by oxygen cutting. However, in the cutting process, a large amount of dust is generated when metal materials and plasma are encountered, mainly containing metal dust and smoke, with the primary soot consisting of spherical particles with a diameter of about 3 micrometers, and the secondary aggregated soot with larger size. The soot can easily enter the human lungs, harming health and polluting the environment. Therefore, dust removal devices must be installed in plasma cutting to protect on-site personnel and the environment while improving product quality [2].

In order to analyze the movement principle of dust in the cutting process and optimize the dust removal effect, scholars in China and other countries have carried out detailed studies. Based on the principle of fluid dynamics, Jiang Huarui [3] simulated the flow direction of dust particles in laser precision cutting, and studied the distribution and trend of smooth and turbulent flow of dust particles in the cavity. Hoover [4] analyzed the cutting materials and found that the processing of brittle materials has a larger median diameter of the mass of dust particles produced than the processing of ductile materials and that the stronger the fracture toughness, the more the material produces the more dust. D. Dekeyser et al. [5] obtained the effect of different airflows on the dust removal effect by setting different flow rates, flow velocities, and fan powers. Ma Yubao [6] focused on optimizing the host airflow of the dust removal system in plasma cutting. Chen Chao [7] discussed the influence of host power and suction port area on the dust removal effect. It can be seen that the influence of the dust removal effect includes the characteristics of material and the process parameters of the exhaust system, and the use of process parameters for optimization is relatively simple and feasible. On the other hand, scholars actively improving the structure of the dust removal device to enhance the dust removal effect. Yingchuang Lv [8] shortened the air duct by setting welded partitions and improved the dust removal speed.Ligui Jiang [9] improved dedusting efficiency by designing a partitioned dedusting system for a large-envelope laser cutting machine with two dampers working simultaneously in the same partition and an axial fan installed on the top cover of the machine guard, which greatly inhibits the diffusion of metal fume into the upper space of the working table. Yanjun Chen [10] combining high-pressure water spraying and dry cartridges, the dust removal system has been modified, which greatly facilitates the cleaning of dust at a later stage.

Received on April 1, 2024; Accepted on May 25, 2024

Danyang Feng [11] The dust removal of fine plasma cutting is improved by increasing the dust removal air volume, adding a side-blowing device, modifying air ducts, and strengthening maintenance. Aiwei Liu [12] optimized the dust removal pipe of the machine tool, the clearance between the workbench and the blanking plate, and the damper control.Guangming Hu [13] et al. designed a special cutting air outlet capturing a vertical table, but the structure occupies a large site area and is not conducive to the automation improvement of the workstation, etc. Zhongwei Wu [14] based on the principle of plasma discharge adsorption to purify welding fume, has developed a dust removal device, which can track the source of welding fumes in real time but is not suitable for cutting large parts such as longitudinal beams. Although it is feasible to improve the dust removal efficiency by increasing the device, it is not suitable for all enterprises that have already installed the completed dust removal system due to the high coefficient of structural difficulty and high modification costs.

This paper optimizes the dust removal system for the cutting longitudinal beam station of an enterprise, proposes a more cost-effective structure improvement scheme, and confirms a better effect of dust removal through simulation and on-site testing, which not only improves product quality and productivity, reduces manpower costs, but also provides a reference to solve the related problems in the industry, which has greater value for market application.

2 Basic Principle of Plasma Dust Removal System

At present, most of Chinese enterprise use wet dust removal methods and dry dust removal methods.

2.1 Method of wet de-dusting

The method of wet de-dusting is to set up a water storage pool under the workstation,the cutting and sparks generated during cutting can automatically fall into the pool, due to the light density of soot，the dust removal efficiency is low.Cutting in water, although the dust removal efficiency of this method is higher, it affects the cutting efficiency and also prolongs the time of auxiliary processes such as loading and unloading, and at the same time, it is easy to cause water pollution.

2.2 Method of dry dusting

Dry dust removal processes typically require the design of a collection system to capture the fumes and dust in the system, which is then transported to the purification equipment and discharged after the treatment is completed. Commonly used collection systems are negative pressure de-dusting systems，also called direct suction systems， and blowing suction de-dusting systems.The negative pressure type dust removal system has more applications, and according to the suction, position can be divided into top suction type and side suction type [15]. Top suction in the cutting table above the negative pressure device, side suction in the table below the negative pressure device, and the opening of the air door around the table, according to the direction of the air door can be subdivided into a single side, double-side, four-side suction system [16], respectively, for with 3 meters or less, 3 meters to 5.5 meters, 2.5 meters or less, and the table is wider.

3 Overall Structural Design of the Dust Removal System

The automotive longitudinal beam is an important supporting structure of the car, and usually needs to be cut by laser or plasma cutting, etc. to obtain the corresponding shape, to meet the appearance and functional requirements of the product. In the traditional dust removal method adopts, the air is sucked out from the top of the room, but the soot easily adsorbs to the lower surface of the longitudinal beam during the rising process, which on one hand affects the quality of the cutting surface, and on the other hand, affects the subsequent painting process, so it is necessary to add a special process to remove the soot.

Now we design a side suction dust removal system located under the table, which is modeled by mechanical software，Siemens NX12. The main structure is shown in Figure 1. One of the dust removal boxes is divided into two layers, the inner box is used to hold the cutting waste inner box, the sandwich between the inner and outer layers of the fume collection channel and along the direction of the main guide rail of the cutting machine is divided into several uniformly closed small areas, the side of the open air outlet, the air outlet is equipped with a horizontal diversion plate above, and the bottom of the upward tilting of the diversion plate, as shown in Figure 2. Each extraction chamber is designed to install a mechanism to open the dampers. By moving the table to trigger the switch, the resulting fumes and dust will be sucked into the air ducts promptly, and directly into the main body of the dust collector for purification. The original ordinary switch model is converted into into a conical damper.

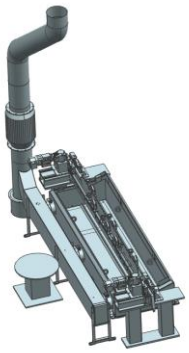

Figure 1 Overall structure of dust removal system

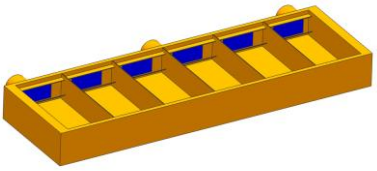

Figure 2 Structure of dust removal box

4 Mathematical Modelling

The process of absorbing dust is a typical turbulent gas-solid two-phase flow composed of moving airflow and ejected dust particles, which is a typical two-phase flow model, Commonly used two-phase flow models include the Volume of Fluid Model, the Mixture Model, and the Eulerian Model. In these models, the Eulerian Model regards each phase as a continuous medium that fills the entire flow field, writes the mass, momentum, and energy conservation equations for the two phases respectively, and couples the two sets of equations together through the interaction between phase interfaces, providing a more comprehensive and widespread method.

Modeling of fluids starts by following the continuity and momentum conservation equations. Due to the anisotropic vortex flow of the gas in the dust removal system, the Reynolds stress model with the assumption of turbulent isotropy is used, and the coupling between the gas and particle phases is solved using the Lagrangian multiphase flow model.

The continuity equation:

$$\frac{\partial(\rho u_x)}{\partial x}+\frac{\partial(\rho u_y)}{\partial y}+\frac{\partial(\rho u_z)}{\partial z}+\frac{\partial \rho}{\partial t}=0 \quad (1)$$

In the formula，u_x，u_y，u_z is the fluid velocity;ρ is the fluid density.

Conservation of momentum equation:

$$\frac{d\vec{V}}{\partial t}=\vec{F}+\frac{1}{\rho}\left(\frac{\partial \overrightarrow{P_x}}{\partial x}+\frac{\partial \overrightarrow{P_y}}{\partial y}+\frac{\partial \overrightarrow{P_z}}{\partial z}\right) \quad (2)$$

In the formula，$\overrightarrow{P}$ is the fluid stress vector, and $\overrightarrow{F}$ is the mass force distribution density.

Reynolds stress equation:

$$\frac{\partial}{\partial t}(\rho\overline{u_\iota u_j})+\frac{\partial}{\partial x_k}(\rho U_k\overline{u_\iota u_j})=D_{ij}+\varphi_{ij}+G_{ij}-\varepsilon_{ij} \quad (3)$$

In the formula，$\frac{\partial}{\partial t}(\rho\overline{u_\iota u_j})$ is the time rate of change of the Reynolds stress, $\frac{\partial}{\partial x_k}(\rho U_k\overline{u_\iota u_j})$ is the convection term, D_{ij} is the diffusion term, andφ_{ij} is the pressure strain term,G_{ij} is the generation term, andε_{ij} is the dissipation term.

Particle equations of motion:

$$\frac{du_p}{\partial t}=F_d(U_I-u_p)+g\frac{(\rho_p-\rho)}{\rho_p} \quad (4)$$

$$\frac{dx_p}{\partial t}=u_p \quad (5)$$

In the formula，x_p is the particle position，ρ_p is the particle density, u_p is the particle velocity

5 Simulation and Experimental Verification

5.1 Model building and meshing

In the dust duct, each small enclosed area is isolated from one another and the dampers are controlled independently. During the cutting process, the nozzle moves at an approximately constant speed, and when the nozzle moves to the corresponding area, the damper in the area opens, so a closed area is modeled as a simulation object, and it is modeled using Siemens NX12 as shown in Figure 3. The damper is set as a pressure outlet, the upper surface is set as the velocity inlet, and all others are walls. The meshing is carried out in ANSYS MESHING in the form of tetrahedral mesh with the number of meshes 330639, as shown in Figure 4.

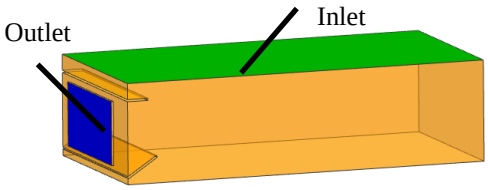

Figure 3 Physical model

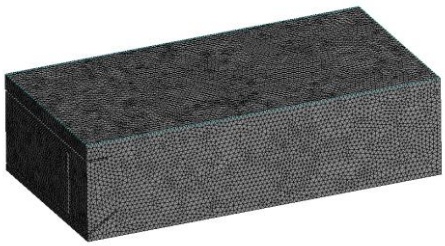

Figure 4 Mesh division

5.2 Model solving

The dust removal process was simulated using FLUENT. The transient simulation is used, the gravitational acceleration is set, the time step of the transient simulation is set to 0.001s, the number of inner iteration steps is set to 20, and the maximum solution time of the transient is 5 s. The gas inlet boundary condition is the velocity inlet with a velocity value of 10m/s, the material is air and the exit velocity is the pressure outlet with a pressure value of -1000 Pa. The particle incidence method is the planar incidence source. and the incident plane is the gas-phase Inlet plane, the material is steel, the incident direction is the dierection normal to the plane, the incident length is 1s, the size of the particles is 3 microns, the incident velocity is 5m/s,

and a total of 8248 particles injected. The particles at the inlet were set to escape and the outlet was set to capture, i.e., the particles were considered to be absorbed when they reached the outlet.

5.3 Simulation results and analysis

The simulated particle movement trajectory is shown in Figure 5. The number of particles captured at the pressure outlet surface is 8202, and the particle collection rate is 99.44%, dividing by the number of captured particles by the number of incident particles. The effectiveness of the dust removal system is proven. The results of the pressure simulation are shown in Figure 6, which shows that the application of the diversion plate effectively reduces the pressure loss, so that the dust removal suction can have a more effective effect on the inlet surface. Meanwhile, as shown in Figure 7, the velocity vector diagram shows that the underlying particles can also be effectively absorbed .

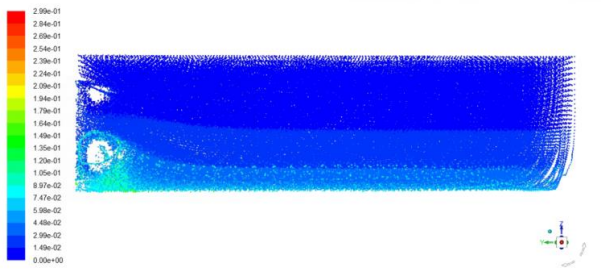

Figure 5 Particle trajectories diagram

Figure 6 Pressure cloud diagram

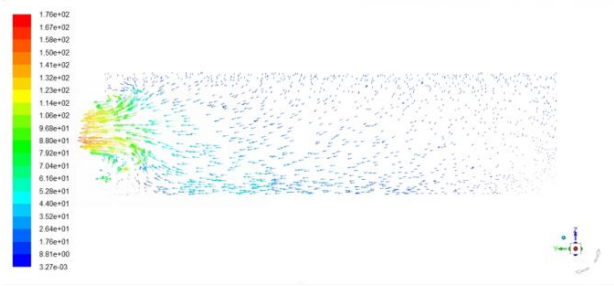

Figure 7 Velocity vector diagram

5.4 Experimental verification

Based on the simulation results, the original upper suction dust removal system was converted into the lower side (Figure 8). The height of the workstation from the ground is 420mm, the thickness is 50mm, the cutting stroke is 2.7m, the track spacing is setted to 1.5m, the height above the ground is 820mm, the waste box dimensions are 2900×800×350mm and the height above the ground is 770mm, the length of the waste box in the middle of the length is 3.3m. After the transformation to carry out the actual test was completed, it was found that the test had a better effect on dust removal.

(a)Before modification (b) After modification

Figure 8 The dust removal system

6 Conclusion

Automotive longitudinal beams are key structural components of automobiles and need to be processed using plasma and other cutting processes. The dust generated during the plasma-cutting process needs to be collected effectively to prevent polluting the environment and damaging the health of employees. This paper A bottom-side suction dust removal system is proposed, using a follower damper with a diversion plate to achieve dust collection. And it is verified that the dust removal rate is higher than traditional method by simulation and field tests, which is of some significance as a guide for similar production modifications. The dust removal method can also explore the blowing and suction combination, the overall pressure adjustment of the workshop and other technologies can also be studied to make further improvement on the dust removal rate.

Funded Project: Changchun Science and Technology Development Plan Project, Automobile Rolling Line Longitudinal Beam Cutting Process Under the Extraction and Dust Removal Process Test and Research, Project Approval No. 21ST04

Author Resume: WenQiang Gao,(1990.1—), Female, Han nationality, Province of Heilongjiang, Intermediate Lecturer, Ph.D., research interests in materials processing engineering.

Reference

[1]Miaosun Chen. Current Situation and Analysis of Plasma Arc Cutting Machine in China[J]. Welding&Joining, 2006(9):23-25.

[2]Renxiang Ding. Development and application of smoke treatment system for plasma cutting machine[J]. China Foundry Machinery & Technology, 2019,54(6):56-58.

[3]Huayue Jiang, Binghai Xiao, Songling Zhang. Research on Flow Field Simulation and Dust Removal Effects of Vacuum Hood of Laser Cutting Equipment[J]. New Technology &

New Process, 2021(1):70-74.
[4]Khettabi R, Songmene V,Masounave J,etal. Under-standing the formation of nano and microparticles during matal cutting [J]. International Journal of Signal System Control and Engineering, 2008, 1(3):203-210.
[5]Dekeyser D,Duga A T,Verboven P,etal.Assessment of orchard sprayers using laboratory experiments and computational fluid dynamics modelling[J]. Biosystems Engineering, 2013, 11(2):157-169.
[6]Yubao Ma, Guoqing Ma. Design and Application of Dust Removal System for Plasma Bevel Cutting [J]. Mechanical Research & Application, 2022, 35(1):101-103.
[7]Chao Chen, Zailiang Chen. Study on the dust produced by laser cutting and dust removal system[J]. China Standardization, 2019(20):247-248.
[8]Yingchuang Lyu, Lu Wang, Shaojun Huang, et al. Improvement of Dust Removal System of CNC Plasma Cutting Machine [J]. Machinery, 2018, 56(12):50-51.
[9]Ligui Jiang, Shukun Cao. Design of a Large Bounding Laser Cutting Machine Partition Dust Removal System [J]. Journal of Shandong Industrial Technology, 2023(3):78-81.
[10] Yanjun CHEN, Junguang MA, Xiaodong ZHANG. Upgrade of Spiral Welded Pipe Plasma Dust Removal Device [J]. Welded Pipe and Tube, 2019, 42(8):43-45+49.
[11]Danyang Feng, Yi Gan, Xinfei Lu. The improved dust removal effect of fine plasma cutting machine In CRRC Zhuzhou Vehicle Co., LTD, The collection in "Yisa Cup" advanced welding technology exchange conference[C]. Beijing: Metal working press, 2021.
[12] Aiwei Liu. Study on dust collector system of laser cutting machine [J]. China Metalforming Equipment & Manufacturing Technology, 2019, 54(6):40-42.
[13]Guangming Hu, Xiaohu Wang, Hongtiao Zhang. Application of dust removal technology in automobile welding and cutting [J]. MW Metal Forming, 2008(14):27-30.
[14] Zhongwei Wu, Jinbing Xia, Xijin Shi. Design and Numerical Simulation of Plasma Welding Fume Removal Devices[J]. China Mechanical Engineering, 2019,30(23):2862-2869.
[15]Wei He. Application of filter dust collector in dust control of CNC plasma cutting machine [J]. MW Metal Forming, 2013(16):28-31.
[16]Qun Wang. Discussion on the application of dust removal device in NC flame plasma cutting [J]. Safety Technology of Special Equipment, 2017(5):58-60.

Viser Technology Pte. Ltd.
Mechanical Engineering Science
DOI: 10.33142/mes.v6i1.13227

Research Article Open Access

Research on Three-Dimensional Simulation of the Internal Arc Gear Skiving

Xiaoqiang WU[1*], Rui XUE[2], Erkuo GUO[3], Dongzhou JIA[4], Taiyan GONG[5], Zengrong LI[5], Haijun YANG[5], Xiaoxue LI[1], Xin JIANG[1,6], Shuai DING[2], Yong LIU[2], Shitian LI[2]

1. School of Mechanical and Traffic Engineering, Ordos Institute of Technology, Ordos, Inner Mongolia, 017000, China
2. Tianjin TANHAS Technology Co .,LTD, Tianjin, 301600, China
3. School of Mechanical Engineering, Jiangsu University, Zhenjiang, Jiangsu, 212002, China
4. College of Mechanical Engineering and Automation, Liaoning University of Technology, Jinzhou, Liaoning, 121001, China
5. Inner Mongolia Ruite Precision Mould Co., LTD., The First Machinery Group, Baotou, Inner Mongolia, 014030, China
6. Inner Mongolia University Of Technology, College Of Energy And Power Engineering, Hohhot, Inner Mongolia, 010051, China

[*]***Corresponding Author:*** *Xiaoqiang WU, E-mail: wangzai8402@163.com*

Abstract

Aiming at the problems that the simulation accuracy which is reduced due to the simplification of the model, a three-dimensional simulation method based on solid modeling is being proposed. By analyzing the motion relationship and positional relationship between the caries knife and the workpiece, the coordinate system of the caries machining was established. With the MATLAB software, the cutting edge model and the blade sweeping surface model of the boring cutter are sequentially established. Boolean operation is performed on the blade swept surface formed by the tooth cutter teeth with time t and the workpiece tooth geometry as well as the undeformed three-dimensional chip geometry model and the instantaneous cogging geometry model are obtained at different times. Through the compare between gear end face simulation tooth profile and the theoretical inner arc tooth profile, we verified the accuracy and rationality of the proposed method.

Keywords: *gear skiving; undeformed three-dimensional chips; solid modeling*

1 Introduction

The application of robots in the food industry, such as in food packaging, sorting, palletizing, canning, automated lunches, and automated cutting (beef), is becoming increasingly widespread. RV reducers is the core components of robots in the food industry, which is known for their strong impact resistance, high torque, high positioning accuracy, low vibration, and high gear reduction ratio. Due to their specialized application conditions, these RV reducers require large specifications, high precision, and impose stringent requirements on the manufacturing processes of their core components.

Scudding technology was named as Skiving or Power Skiving in abroad, which is an emerging gear machining technology in the 21st century [1]. It is highly efficient and precise, particularly suitable for machining non-through internal helical gears and high-precision non-involute gears using dry cutting methods [2].

Scholars at home and abroad utilize professional CAD/CAM/CAE applications to achieve simulation processing of power skiving and extraction of three-dimensional undeformed chips. Antoniadis [1-3] and others utilize the three-dimensional finite element software Abaqus to establish robust power skiving models and conduct finite element cutting simulations of the power skiving process. The simulation models reveal the direction of chip flow, showing good correlation between simulated and actual chips generated during machining. However, the accuracy of gear tooth profiles is relatively low, indicating significant discrepancies compared to real power skiving processes. Liu Bing [4-5] and his colleagues established gear tool geometry models which is based on gear meshing principles and obtain preliminary simulation data using DEFORM-3D software. The simulation accuracy is noted to be relatively low and it belongs to the exploration stage of gear machining.Yang Tangjun [6-7] and others utilize Vericut simulation software for geometric simulation of pre-angle power skiving cutter cutting processes. This approach provides an intuitive view of the three-dimensional geometric shape of gear teeth slots after power skiving. Nevertheless, issues such as improper tool design contribute to significant undercuts and overcuts, resulting in considerable disparities

Received on May 19, 2024; Accepted on June 2, 2024

between simulation results and real power skiving processes. Zhao Haiyang [8] and his collaborators used numerical control simulation technology to construct a virtual simulation power skiving machine model. They achieve geometric simulation of the power skiving process and validate the correctness of the machine-tool movement relationship through Boolean operations to obtain undeformed chip shapes. However, precise analysis of gear profile machining results is not conducted.

At Harbin University of Science and Technology, Li Zhenjia [9-12] and others developed a chip breakage prediction system using the VisualC++6.0 development platform and OpenGL graphics language. They successfully extract three-dimensional undeformed chips. However, the chips extracted exhibit significant differences compared to those obtained from actual machining processes. Dimitriou [13-14] and colleagues implemented a power skiving simulation system to extract undeformed chips. Nonetheless, there is obvious deviation between predicted dynamic power skiving cutting forces and real observations.

Based on the above cases, this paper proposed a three-dimensional simulation method based on solid modeling which not only generates instantaneous tooth slot geometries that closely resemble those from actual power skiving processes but also extracts three-dimensional undeformed chips that closely approximate real-world power skiving results. This approach gets a solid foundation for research into the cutting mechanisms of power skiving, contributing significantly to the advancement of this machining technique.

2 Simulation Part

2.1 Three-dimensional simulation process of gear skiving

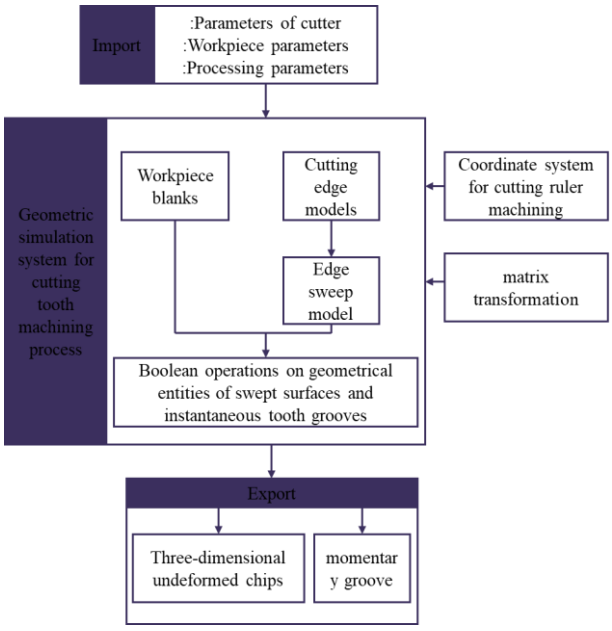

Figure 1 Three-dimensional simulation process of gear skiving

Figure 1 shows the three-dimensional simulation process of Gear Skiving based on solid modeling. After inputting the machining parameters, the simulation system automatically creates the geometric entity of the workpiece and constructs the cutting edge model. The cutting sweep surface model is determined based on the motion and positional relationships between the skiving and the workpiece. The workpiece blank is combined with the cutting sweep surface, and Boolean operations between the cutting sweep surface and the geometric entity of the instantaneous tooth slot form undeformed chips and new instantaneous tooth slots. After simulation completion, three-dimensional models of undeformed chips removed during the cutting process and instantaneous tooth slots are outputted.

2.2 Modeling of Ggear Skiving movement

Figure 2 shows the Gear Skiving coordinate system. Coordinate system $S_1(o_1, x_1, y_1, z_1)$ represents the workpiece coordinate system, while coordinate system $S_2(o_2, x_2, y_2, z_2)$ represents the tool coordinate system. $S_p(o_p, x_p, y_p, z_p)$ and $S_0(o, x, y, z)$ are auxiliary coordinate systems of $S_1(o_1, x_1, y_1, z_1)$ and $S_2(o_2, x_2, y_2, z_2)$, respectively. Coordinate system $S_1(o_1, x_1, y_1, z_1)$ is used to establish the workpiece tooth surface model, and coordinate system $S_2(o_2, x_2, y_2, z_2)$ is used to establish the tool model. Coordinate system S_p serves as an auxiliary system for S_1, and coordinate system S_0 serves as an auxiliary system for S_2, with fixed spatial positions for Sp and S_0. The center distance refers to the perpendicular distance between the tool axis and the workpiece axis, while the axis crossing angle refers to the angle between the tool axis and the workpiece axis. Table 1 presents the Gear Skiving process parameter table.

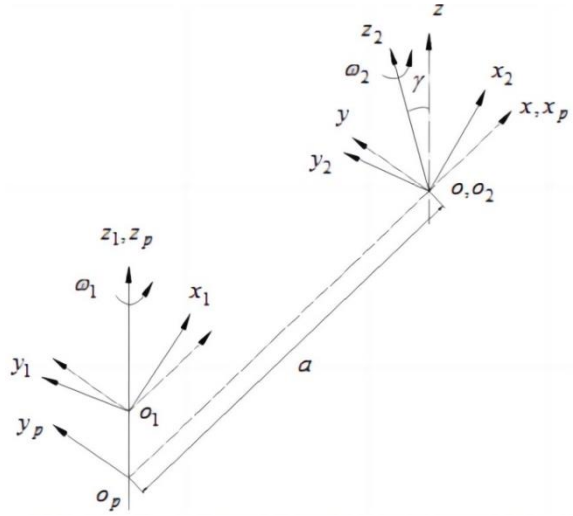

Figure 2 Gear Skiving coordinate system

According to the skivingbing coordinate system shown in Figure 2,the total transformation matrix from the tool coordinate system to the workpiece coordinate system is:

$$T_{20}=\begin{bmatrix}\cos\varphi_1 & -\sin\varphi_1 & 0 & 0\\ \sin\varphi_1 & \cos\varphi_1 & 0 & 0\\ 0 & 0 & 1 & 0\\ 0 & 0 & 0 & 1\end{bmatrix} \quad (1)$$

$$T_{op}=\begin{bmatrix}1 & 0 & 0 & 0\\ 0 & \cos\gamma & -\sin\gamma & 0\\ 0 & \sin\gamma & \cos\gamma & 0\\ 0 & 0 & 0 & 1\end{bmatrix} \quad (2)$$

$$T_{p1}=\begin{bmatrix}\cos\varphi_2 & \sin\varphi_2 & 0 & 0\\ -\sin\varphi_2 & \cos\varphi_2 & 0 & 0\\ 0 & 0 & 1 & 0\\ 0 & 0 & 0 & 1\end{bmatrix} \quad (3)$$

In the formula, T_{20} denotes the transformation matrix from the tool coordinate system S_2 to the auxiliary coordinate system S_0, T_{op} denotes the transformation matrix from the auxiliary coordinate system S_0 to the auxiliary coordinate system S_p, and T_{p1} denotes the transformation matrix from the auxiliary coordinate system Sp to the workpiece coordinate system S_1.

The theoretical tooth surface of the cutting edge conforms to a conjugate relationship with the workpiece. The intersection obtained by intersecting a plane with the conjugate surface yields the cutting edge. By utilizing numerical discretization method combined with the process parameters in Table 1, the cutting edge of the skiving can be obtained. The three-dimensional simulation result of the cutting edge using MATLAB software is shown in Figure 3.

Based on the motion and positional relationships between the skiving and the workpiece, the cutting sweep surface model can be obtained. The three-dimensional simulation result of the cutting sweep surface using MATLAB software is shown in Figure 4.

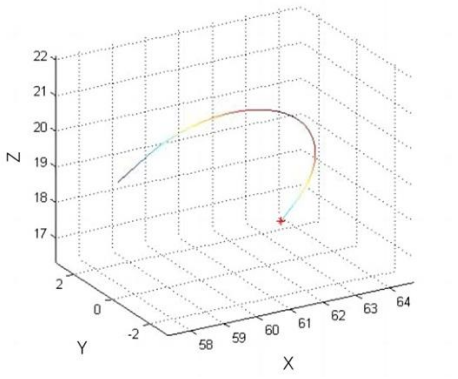

Figure 3 Simulation result of the cutting edge in MATLAB

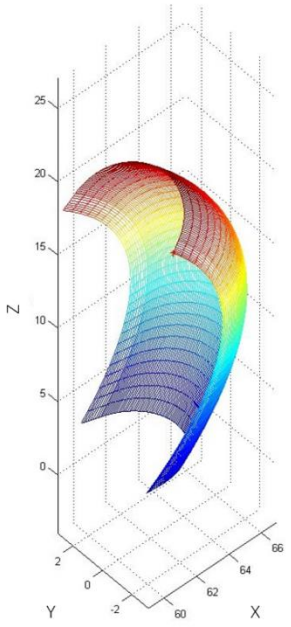

Figure 4 Three-dimensional simulation result of the cutting sweep surface

Table 1 Gear Skiving Process Parameters

Parameter type	Parameter Descriptions	Parameter Value
Cutting knife parameters	Knife teeth	22
	Knife helix angle	20 °
	Knife arc radius	5.8
	Knife pitch diameter	128
	γ_o Knife cutting front edge angle γ_o	5 °
	α_d Knife designing back angle α_d	6 °
Workpiece parameters	Teeth of workpiece	40
	helix angle of workpiece	0
	teeth width of workpiece	60
Machining parameter	Center distance	26.4525
	Axis crossing angle	20 °
	(mm/r)Axial feed rate/(mm/r)	0.15
	(r/min)Knife rotation speed/(r/min)	700
	(r/min) Workpiece rotation speed/(r/min)	385

2.3 Implementation of three-dimensional simulation process for Gear Skiving movement

In Gear Skiving, the radial direction is divided into multiple cutting layers for machining. The final accuracy of the tooth surface is ensured by the cutting process corresponding to the last radial feed. Therefore, this paper selects a cutting depth of 0.03mm for the final pass to discuss the machining process.

The three-dimensional simulation of Gear Skiving movement primarily involves removing workpiece material by Boolean operations between adjacent cutting sweep surfaces formed by successive skiving teeth over time t and the instantaneous tooth slots. The material removed from the workpiece constitutes the undeformed three-dimensional chips.

During Gear Skiving, the cutting sweep surface formed by a single skiving tooth over time t can only machine a portion of the tooth surface on the workpiece. To complete the entire tooth width, an axial feed motion is required. After a single skiving tooth completes a cutting pass with its cutting sweep surface over time t, upon the workpiece rotating one full revolution, another skiving tooth forms a cutting sweep surface over time t to continue machining the same workpiece tooth slot.

As shown in Figure 5, the subsequently formed cutting sweep surface translates forward along the tooth direction of the workpiece under axial movement. The material at the intersection between this cutting sweep surface and the previously machined tooth surface is removed, gradually shaping the machined tooth surface closer to its theoretical shape. This cyclic process repeats multiple times with cutting sweep surfaces formed by successive skiving teeth over time t, collectively completing the machining of the workpiece tooth surface.

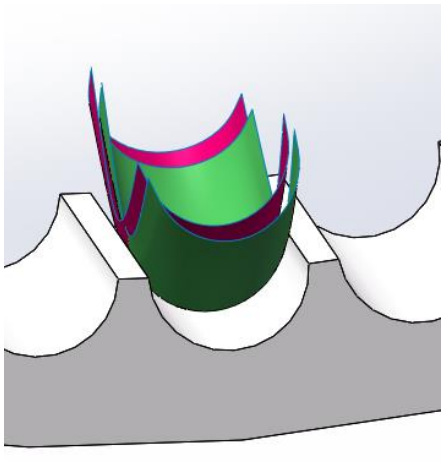

Figure 5 Schematic of the tooth surface formation process in Gear Skiving

Taking the j cutting sweep surface as an example, the undeformed three-dimensional chip is obtained by performing Boolean operations (difference and intersection) between the j-i cutting sweep surface and the j cutting sweep surface with the instantaneous tooth slot. Thus, the undeformed three-dimensional chip obtained after the j cutting sweep surface and its corresponding instantaneous tooth slot are shown in Figure 6.

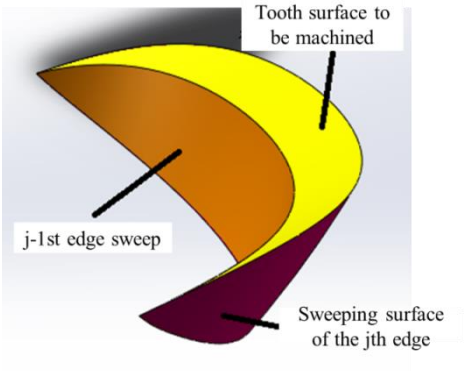

(a) Undeformed three-dimensional chips

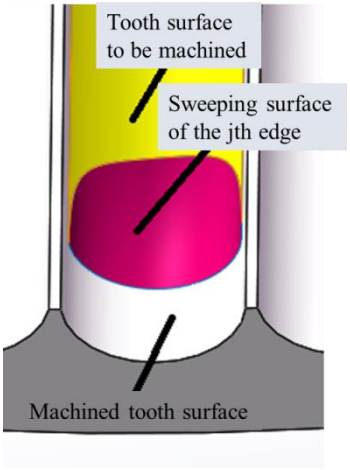

(b) Instantaneous tooth groove

Figure 6 Boolean operations between adjacent cutting sweep surfaces and the workpiece

3 Mulation Example and Result Analysis

The skivingbing tool employs an internal circular arc skiving, using internal spur gears as an example. Parameters are selected based on Table 1.

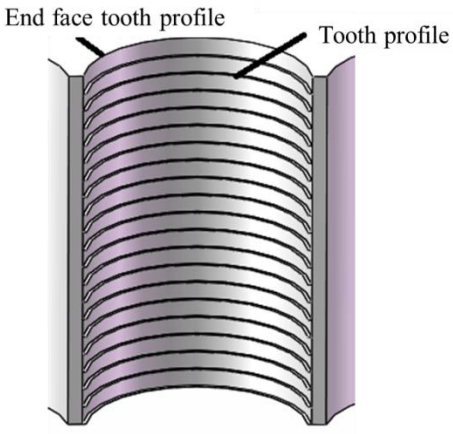

Figure 7 Simulated gear profile

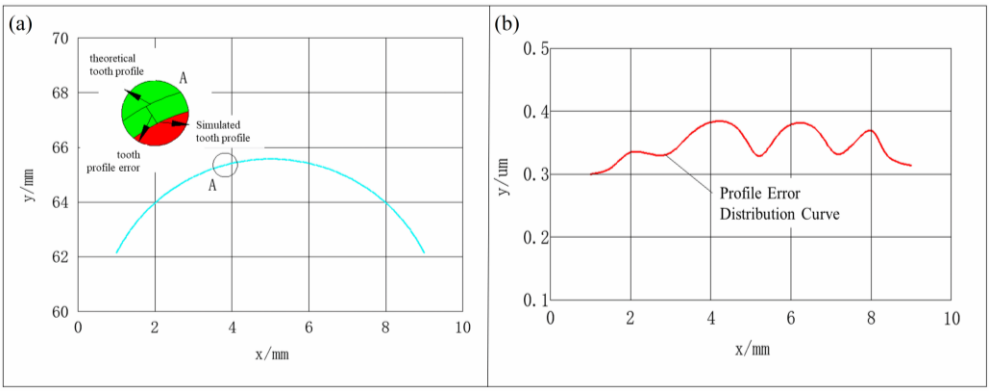

Figure 8 Simulated gear profile and its error:(a) Simulated gear profile and theoretical gear profile;(b) Gear profile error distribution curve

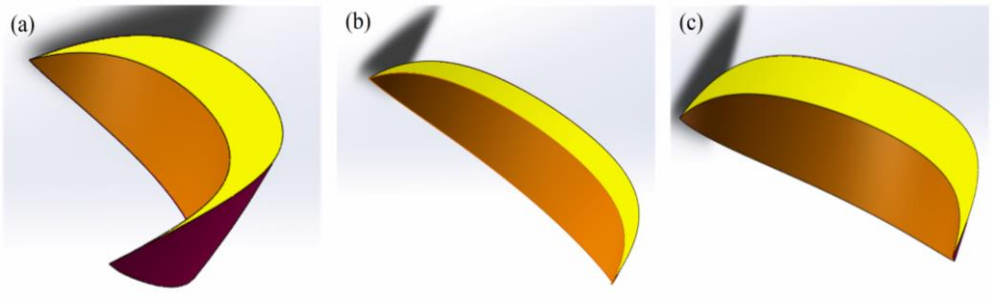

Figure 9 Three-dimensional undeformed chips at different time instants

Figure 7 shows the profile of the internal spur gear formed after simulation processing. Data points of the gear tooth profile extracted in the SolidWorks secondary development environment were subjected to curve fitting in MATLAB software. Figure 8(a) presents a schematic comparison between the simulated gear profile curve after fitting and the theoretical involute gear profile curve. The profile error distribution curve is depicted in Figure 8(b), showing the truncation error distribution of a skiving tooth without introducing artificial measurement errors. The error values are controlled within the range of 0.3μ~0.4μ, indicating the accuracy and rationality of the simulation method adopted in this study. Figure 9 illustrates the three-dimensional time t undeformed chips formed by the cutting sweep surfaces of different skiving teeth at various time instants.

4 Conclusion

Aiming the issue of reduced simulation accuracy due to model simplification, this paper proposes a three-dimensional simulation method based on solid modeling. The method involves performing Boolean operations between the cutting sweep surface formed by the skiving tooth over time t and the instantaneous tooth slot, thereby obtaining the geometric models of the instantaneous tooth slot and the undeformed three-dimensional chip. The comparison between the simulated gear's end face profile and the theoretical involute gear profile yields an error range of .3μ～.4μ, indicating reasonable accuracy of the proposed method.

The gear profile formed by simulation, after surface modeling, generates a three-dimensional geometric model of the gear that is useful for analyzing gear contact characteristics. The undeformed three-dimensional chips formed by simulation will provide a foundation for studying the dynamic cutting forces of skivingbing, as well as the cutting mechanics such as skiving wear.

Fund Projects: The National Natural Science Foundation of China (No. 52165060,12272189), Program for Young Talents of Science and Technology in Universities of Inner Mongolia Autonomous Region:(NJYT23022);Science and Technology Projects of Inner Mongolia Autonomous Region:(2021GG0432);Central Guiding Local Science and Technology Development Plan (2022ZY0013); Basic research business fee project for universities directly under Inner Mongolia Autonomous Region (GXKY22046).

References

[1] Antoniadis A, MATHE P. Development of a General Tool Model for Turning Operations Based on a Variable Flow Stress Theory[J]. International Journal of Machine Tool &Manufacturing, 1995,35(1):71-90.

[2] Antoniadis A. On the Controllabitity of Chip Breaking Cycles and Model of Chip Breaking in Metal Maching[J]. Annals of the CIRP, 1990,39(1):47-51.

[4] Antoniadis A, Arai M. Comprehensive chip form classification based on the cutting mechanism.Annals of the CIRP, 1992,41(1):71-74.
[5] Liu B. Simulation and analysis of gear skivingbing process[D]. Xi'an: Xi'an University of Technology, 2014.
[6] Liu B. Current development status of gear skivingbing technology[J]. Tool Technology, 2014(22)35-39.
[7] Yang. Design of pre-skiving skiving with lead angle. Master's thesis[D]. Tianjin:Tianjin University, 2016.
[8] Li J, Yang T, Wang P, et al. Calculation method for design of pre-skiving skiving[M]. beijing:Mechanical Science and Technology, 2016.
[9] Zhao H. Analysis of gear skiving process and kinematic simulation[D]. Xi'an:Xi'an University of Technology, 2016.
[10] Li Z, Zheng M, Wei Y, et al. Study on chip spatial motion trajectory and its constraint equations[J]. Journal of Mechanical Engineering, 2001,37(12):42-46.
[11] Zhang Z, Li Z, Zheng M, et al. Theoretical study on chip breaking limit[J]. Journal of Mechanical Engineering, 2002,38(8):74-79.
[12] Li G, Li Z, Chang Z. Simulation of chip formation process[J]. Journal of Heilongjiang Institute of Technology, 2002,16(1):27-29.
[13] Liu E, Li Z, Yan F, et al. Study on cutting aluminum alloy chips with PCD tools[J]. Journal of Harbin University of Science and Technology, 2003,8(2):1-4.

Viser Technology Pte. Ltd.
Mechanical Engineering Science
DOI: 10.33142/mes.v6i1.13228

Research Article Open Access

Design a Special Fixture for Tractor Lever

Guanghui LI, Yongliang YUAN*

He'nan Polytechnic University, He'nan, Jiaozuo, 454150, China

***Corresponding Author:** *Yongliang YUAN, E-mail: yuan-yong-liang@163.com*

Abstract

Aiming at the problems of long time and poor machining precision in processing the tractor lever workpiece, a special fixture suitable for the tractor lever workpiece is designed by analyzing the processing technology of the lever workpiece, and the workpiece is accurately positioned and tightened under the action of the special fixture. Efficient machining of the workpiece can be achieved by using a drill template. The fixture not only has the advantages of high production efficiency, low cost and high life, but also effectively improves the processing technology of the workpiece, and has certain reference value for the subsequent fixture improvement design.

Keywords: *tractor lever; special fixture; drill template*

1 Introduction

1.1 Classification of fixtures

Machine tool fixtures according to the use of machine tools can be divided into lathe fixtures, milling machine fixtures, drilling machine fixtures, boring machine fixtures and grinding machine fixtures. Machine tool fixtures according to its general characteristics can be divided into general-purpose fixtures, special fixtures, adjustable fixtures, combined fixtures and production line fixtures, mainly reflecting the characteristics of the fixtures in different types of production.

1.2 Introduction to specialized fixture

Specialized fixtures are designed and manufactured for a certain process of machining parts, they are used in the production of relatively stable products and large batches. Special fixtures can effectively reduce the labor intensity at work, improve labor productivity, and obtain higher machining accuracy. These fixtures are usually composed of positioning elements, clamping devices, tool guidance elements, indexing devices, connecting elements and clamping specific, for a certain kind of product parts in a certain process of clamping needs to be specially designed and manufactured, the object of the service is dedicated to a very strong target.

Specialized fixtures of various types, including but not limited to lathe fixtures, milling machine fixtures, drilling molds, boring molds and fixtures with the line. These fixtures can be used to replace or adjust components as needed, and consist of standardized components of different shapes, sizes, and uses, and are suitable for single-piece, small-batch production of new products for trial production and frequent product replacement, as well as for temporary tasks. Machine tool fixture is an indispensable process equipment in modern production, which directly affects the precision of processing, labor efficiency and product cost.

1.3 Research status of specialized fixtures

The research of special fixtures is involved both at home and abroad, mainly including the following aspects: design optimization and intelligence, material and manufacturing technology, flexible fixtures, digital technology application, standardization and normalization.

For different workpieces and production requirements, researchers are committed to optimizing the design of fixtures so that they can improve productivity and machining accuracy. At the same time, through the introduction of sensors, control systems and machine learning and other technologies, to realize the intelligence of the fixture, so that it can adapt to different workpieces and machining conditions. In addition researchers are exploring new materials and manufacturing technologies to improve the performance and durability of fixtures.

With the change of production demand and the increase of personalization, flexible fixtures have become one of the hot spots of research. This kind of fixture has a strong adaptive ability, can quickly adjust and adapt to the shape and size of different workpieces,

Received on May 11, 2024; Accepted on June 7, 2024

so to improve the flexibility and efficiency of the production line. Digital technology is also widely used in the research of special fixtures. These technologies can help engineers design and optimize fixtures, identify potential problems in advance, and optimize the production process. And in order to improve the interoperability and universality of fixtures, some international organizations and standardization agencies are also promoting the standardization and normalization of special fixtures to promote technical exchanges and cooperation within the industry. In general, the research status of special fixtures is constantly developing in the direction of intelligence, flexibility and digitization, aiming to meet the increasingly complex production needs and improve production efficiency [1-4].

1.4 Specia fixture for tractor lever

The primary function of lever parts is to support and secure components; and they are one of the core components of tractor engines. With nation's increasing emphasis on agriculture, and considering that tractors are crucial machinery and equipment in agricultural production, so the demand for lever parts has gradually increased. To address the issue of multiple processes in lever parts, multifunctional fixtures have been adopted internationally for clamping workpieces, and they have already been applied on CNC machine tools. However, due to the typically high costs of multifunctional fixtures, their demand remains relatively low among small and medium-sized enterprises. In nation's small and medium-sized enterprises, products are usually processed using a multi-process, multi-fixture approach.

For certain processes, specialized fixtures are often used for clamping and machining workpieces to reduce auxiliary processing time and improve machining accuracy [5-8]. Considering the characteristics and precision requirements of tractor lever workpieces, a set of specialized fixtures has been designed to achieve efficient and cost-effective machining, thereby meeting the product's precision requirements.

2 Analysis of Lever Workpieces

2.1 The importance of tractor levers

Special fixture for tractor levers has a great role in the field of agricultural machinery. Tractor levers are one of the key components of the tractor, and their quality and precision directly affect the performance and lifetime of the tractor. The use of special fixtures can ensure the machining accuracy and consistency of the lever, thus improving production efficiency and reducing human errors and losses in the production process.

Specialized fixtures can ensure stable clamping of tractor levers during machining, avoiding machining errors and quality problems caused by unstable clamping. Through accurate clamping and positioning, the size and shape of the lever can be ensured to meet the design requirements, thus ensuring the quality of the product. Although the design and manufacture of specialized fixtures may require a certain cost investment, the total production cost can be reduced by improving productivity and product quality, which can reduce the scrap rate and rework rate during the production process. Specialized fixtures can reduce the risk of accidental injury by reducing direct worker contact during the machining process. Through automated clamping and machining, the safety of the work environment can be improved and the health of workers can be protected. Therefore, special fixtures for tractor levers are important in improving production efficiency, ensuring product quality, reducing production costs and enhancing worker safety, and have a positive impact on the development of agricultural machinery manufacturing enterprises [9-10].

2.2 Structural shape of the tractor lever

The structural shape of a tractor lever can vary depending on the model and function, but it usually has the following characteristics: body part, connecting joint, supporting structure, adjusting device, and surface treatment.

Body part: the body of a tractor lever is usually a long or curved shaped member that connects to the frame or other parts of the tractor and transmits force or carries a load. Connecting Joints: Tractor levers usually have connecting joints that are used to connect the lever to other components such as a trailer, implement or hitch. These connecting joints may be ball joints, pins, threaded connections, or other forms. Supporting structures: In order to increase the strength and stability of the lever, supporting structures such as stiffeners, braces or frames may be added to the structure of the lever. Adjustments: Some tractor levers have adjustments that allow the length or angle of the lever to be adjusted to suit different work requirements or terrain conditions. Surface treatment: Tractor levers are often given a surface treatment, such as spray coating, galvanizing or anodizing, to improve their corrosion resistance and cosmetic quality.

The part structure and shape of the lever of a certain model of tractor are shown in Figure 1. It is made of QT400-18 casting, which has good machinability and can withstand certain impacts and vibrations. Based on the part requirements, the main processes that need to be machined include: Rough and finish milling of the upper and lower platforms with a width of Φ40mm, drilling a Φ10 (H7) hole, drilling of 2×Φ8 holes, and rough and finish milling the upper and lower surfaces of the Φ30 tabs. Based on the requirements of the lever workpiece, the traditional machining process scheme is shown in Table 1. It mainly includes milling, drilling, and reaming to ensure the machining accuracy of the workpiece. During the milling and drilling processes, a set of fixtures is usually modified or combined to ensure machining

Table 1 Tractor lever machining process plan

Operation number	Operation content
05	Rough and finish milling of the upper and lower platforms with a width of 40mm
10	Rough and finish milling of the convex surface with a width of Φ30mm
15	Drill hole Φ25 (H9) to achieve a size of Φ23mm
20	Reaming to enlarge the hole from Φ25 to Φ24.8mm
25	Reaming Φ25 to achieve a size of Φ25 (H9)
30	Drilling a Φ10 hole to achieve a size of 9.8mm
35	Rough reaming the Φ10 hole to achieve a size of 9.96mm
40	Finish reaming the Φ10 hole to meet the requirements.
45	Drilling, rough reaming, and finish reaming 2×Φ8 holes to meet the requirements.

quality. In mass production, this not only causes excessive labor intensity but also makes it difficult to preserve the fixtures [11]. Additionally, the repeated use of fixtures results in a decline in their accuracy, thereby reducing the quality of the lever products.

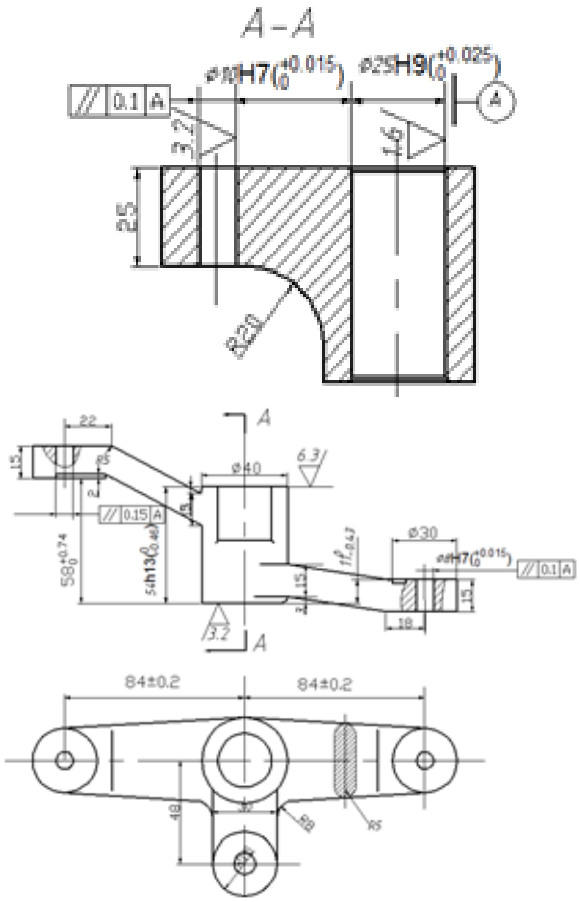

Figure 1 Tractor Lever Part Drawing

3 Scheme Selection and Error Calculation

3.1 Positioning scheme and selection of positioning elements

To ensure proper positioning of the workpiece, in this design, Φ25 and the horizontal plane bottom, as well as Φ30 boss, are selected for positioning. To prevent deformation of the workpiece during drilling of Φ8 (H7) mm holes, a spiral auxiliary support is used. When the auxiliary support contacts the workpiece, it is tightened with a nut.

To prevent phenomena such as rotation during machining, rotation is locked using a nut, thus limiting its six degrees of freedom. At the same time, the option of adding auxiliary support to prevent deformation of the workpiece during machining [12].

3.2 Calculation of positioning error

In the drilling process, in order to ensure that the coaxiality of the holes in the drilling process meets the requirements, so it is necessary to calculate the positioning error of this program. According to the principle of datum coincidence, the positioning error of this fixture is: 0.015+0.015=0.03mm, and the datum displacement error is: 0.052+0.052mm=0.104mm; combining with the accuracy requirements of the positioning holes in the parts diagram, it can be seen that 0.03+0.104mm=0.134＜0.15mm, so it can be seen that the positioning accuracy of this special fixture can Therefore, it can be seen that the positioning accuracy of this special fixture can meet the requirements.

4 Fixture Design

4.1 Fixture design process

The fixture design process usually includes the following steps: requirement analysis, conceptual design, detailed design, material selection, manufacturing and assembly, testing and commissioning, use and maintenance.

First, it is necessary to communicate with the customer or production department to understand the needs and technical requirements for the use of the fixture. This includes the type, size and shape of the workpiece to be clamped, as well as the special requirements of the production process. After the needs

are clarified, a preliminary conceptual design is carried out. This stage usually consists of sketches, hand-drawn or CAD drawings, which are used to explore possible fixture forms and configurations, as well as to define basic clamping principles and schemes. After the conceptual design has been finalized, detailed design work is carried out. This includes developing the detailed structure, dimensions and materials of the fixture, and considering specific details of the fixture's mechanics, clamping methods, and positioning to ensure that the fixture meets the design requirements and performs well. Selection of suitable materials according to design requirements and usage environment. Fixtures are usually made of metal materials such as steel, aluminum, and so on, and special surface treatments or coatings may also need to be considered to improve durability and corrosion resistance. After completing the design, the manufacturing and assembly of the fixture is carried out. This includes machining of the fixture components, heat treatment, surface treatment, assembly and other processes to ensure that the components of the fixture meet the design requirements and are able to function properly. After the completion of manufacturing, the fixture test and debugging work. This includes checking the functions and performance of the fixture to ensure that the fixture can clamp the workpiece stably and accurately and meet the production requirements. Finally, the fixtures are put into service and a maintenance program is established accordingly. The fixtures are regularly inspected and maintained to ensure proper functioning, and adjustments or improvements are made as needed [13-15].

4.2 Structural design of the fixture

The structural design of a fixture is a critical step in ensuring that the workpiece is held securely and machined accurately. First of all, according to the shape, size and machining requirements of the workpiece, determine the clamping method of the fixture. Common clamping methods include mechanical clamping, pneumatic clamping, hydraulic clamping and so on. Selecting the appropriate clamping method can improve the stability and accuracy of the fixture.

Then determine the clamping point and clamping force of the fixture to ensure that the workpiece can be firmly clamped, and will not damage the surface of the workpiece due to excessive clamping force. The structure of the fixture is designed according to the requirements of the clamping method and clamping force. This includes the main structure of the fixture, the layout and configuration of the fixture's clamping components, and the fixture's support and positioning structures. When designing the fixture structure, the requirements of the machining process need to be taken into account. For example, if the workpiece needs to be machined on multiple sides, the structure of the fixture needs to take into account the turning and positioning of the workpiece.

Next, select the appropriate material and surface treatment to ensure that the fixture has sufficient strength, rigidity and durability. Common fixture materials include steel and aluminum alloys, and surface treatments include coating, chrome plating, and nitriding[16].

Finally, in the process of fixture structure design, the operator's use habits and safety requirements are taken into account to design reasonable fixture operating handles, adjusting devices and protection devices to improve the operator's work efficiency and safety. Verify the structural design of the fixture through computational analysis, digital simulation or physical model to ensure that the fixture can meet the requirements of workpiece processing, and has sufficient stability and accuracy. Fixture structure design is a continuous improvement process. During the use of the fixture, feedback information is constantly collected, and the fixture is adjusted and improved according to the actual situation in order to improve the performance and efficiency of the fixture.

Through the analysis of the workpiece, it can be seen that Φ8 holes are relatively small, the quality of the blank parts is relatively small, in order to facilitate mass production and suitable for small and medium-sized enterprises low-cost requirements, so in this design will be designed as a fixture for the flip-type drilling mold mode[17-19].

In order to meet the requirements of the two Φ8 holes and address the shortcomings of traditional methods, a set of specialized fixtures has been designed. This fixture primarily utilizes auxiliary support for positioning the lever, thus enabling adjustment of the cutting forces generated during machining. It mainly consists of components such as a drilling template, locating pins, fixture body, and drill sleeves. To enhance the durability and accuracy of the specialized fixture, Q235 material is used for its design. A schematic diagram of the fixture is shown in Figure 2.

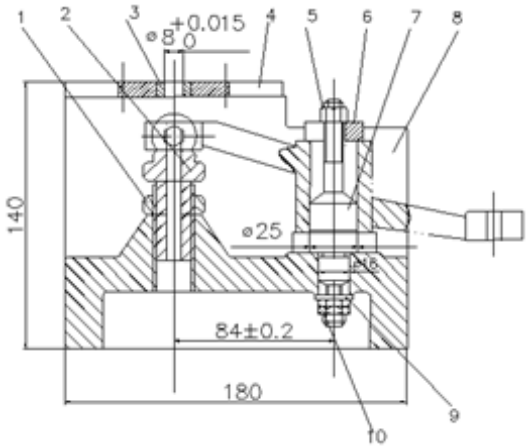

1- Locking nut; 2- Spiral auxiliary support; 3- Drill sleeve; 4- Drilling template; 5- Tightening nut; 6- Open washer; 7- Locating pin; 8- Fixture body; 9- Screw; 10- Locking nut

Figure 2 Schematic diagram of specialized fixture

Through the design and manufacture of the special fixture, and the use of automation to assist the clamping. After the test in the workshop, the quality and precision of the processed workpieces have been greatly improved, and the qualification rate of the products is as high as 99.2% or more, so the design of the fixture meets the demand of the generation; at the same time, the special fixture has the advantages of low cost, high efficiency, and low labor intensity, which can be popularized in the small and medium-sized enterprises and realize mass production.

5 Conclusion

Taking into account the long processing time and poor machining accuracy encountered during the machining of lever components for a certain model of tractor, a specialized fixture has been designed. After the physical inspection in the workshop, the fixture is safe and reliable, and significantly increase the production efficiency. Considering to reduce the number of special fixtures for small and medium-sized enterprises, this fixture still has a large optimization space, which is an important reference value for the optimization of special fixtures in the future.

Fixture design has a broad development outlook in the future, which is mainly reflected in the following aspects: intelligence and digitalization, flexibility and customization, lightweight and composite materials, augmented reality and virtual simulation, environmental protection and sustainable development.

With the development of artificial intelligence, IoT and digital technology, fixture design will become more intelligent and digital. Fixtures will be equipped with sensors and control systems that can monitor the status of the workpiece and machining parameters in real time and make adaptive adjustments based on real-time data to achieve more efficient and accurate machining.

Future fixture design will pay more attention to flexibility and customization, can quickly adapt to different workpieces and production needs. Through modular design and programmable control, the fixture can be flexibly adjusted to adapt to different workpiece shapes, sizes and machining processes, thus improving the flexibility and adaptability of the production line.

Future fixture design will pay more attention to lightweight and material innovation. The use of lightweight materials and composite materials manufacturing fixtures can reduce the weight and inertia of the fixture, improve the speed and accuracy of robot clamping, while reducing energy consumption and environmental pollution.

Augmented reality and virtual simulation technologies will be widely used in the fixture design process. Designers can use augmented reality technology to design and debug fixtures in a realistic environment to improve design efficiency and accuracy; at the same time, virtual simulation technology can help designers design and optimize fixtures in a computer-simulated environment to reduce the cost of experimentation and trial and error [20].

Future fixture design will pay more attention to environmental protection and sustainable development. The use of environmentally friendly materials and clean production technology to manufacture fixtures to reduce energy consumption and waste emissions; at the same time, the design of fixtures will take into account the recyclability and recycling of materials to reduce resource waste and environmental pollution.

Fund Projects: This research work was supported by the Henan Natural Science Foundation (No. 222300420168), the Natural Science Foundation of Henan Polytechnic University (B2021-31), Fundamental Research Funds for the Universities of Henan Province (No. NSFRF220415).

References

[1] Rahul R, Laurence N, Briac C, et al. Design and position control of a robotic brace dedicated to the treatment of scoliosis[J]. Robotica, 2023,41(5):1466-1482.

[2] Parvaz H, Hosseini V S. Analysis of reaction forces in fixture locating points: An Analytical, numerical, and experimental study[J]. Proceedings of the Institution of Mechanical Engineers, Part B: Journal of Engineering Manufacture, 2024,238(6-7): 809-822.

[3] V. O, S. A, N. M, et al. Fatigue Testing Approach Utilising Machining Cutting Forces and Fixture Design[J]. Experimental Mechanics, 2024, 64(6):963-968.

[4] Zhen Z, Shancong M, H. J H, et al. Convex relaxation for optimal fixture layout design[J]. IISE Transactions, 2023,55(7):746-754.

[5] Yawen Y, Lei T, Xi C, et al. Design of variable stiffness fixture for computerized embroidery machine based on shape memory polymer[J]. Journal of Intelligent Material Systems and Structures, 2022,33(17):2147-2160.

[6] Junjin M, Yunfei L, Dinghua Z, et al. Dynamic characteristic reconfiguration of a fixture-workpiece system for vibration suppression in milling of thin-walled workpieces based on MR damping fixture[J]. The International Journal of Advanced Manufacturing Technology, 2022,122(9-10):3751-3768.

[7] Kuigang Y, Xianjin W, Weili P. Robust locating research of welding fixtures for the aluminum alloy sidewall of a high-speed train body[J]. The International Journal of Advanced Manufacturing Technology, 2022,122(7-8):3379-3392.

[8] Azuddin M, Jen H Y, Hau C T, et al. Fixture Design for Outer Skin Aircraft Door Manual Drilling Operation with Finite Element Analysis and Ergonomic Consideration[J]. Advances in Materials Science and Engineering, 2022.

[9] Deepak D S, Aditya S S, Vijet B, et al. Design and Analysis of Vibration Fixture for Aerospace Heat Exchanger[J]. Journal of Vibration Engineering & Technologies, 2023,12(4):5609-5624.

[10] Yi H, He Y. Machining process rules for connecting rod

parts and special fixture design[J]. Journal of Physics: Conference Series, 2020,1654(1):12052.
[11] Guozhi D, Yufeng W, Songmei Y, et al. Research on Rapid and Accurate Fixture Design for Non-Intervention Machining of Complex Parts[J]. Metals, 2022,12(7):1174-1174.
[12] Han W. MORNSUN series DC-DC power module test fixture design[J]. Journal of Physics: Conference Series, 2022,2290(1):55-61.
[13] H R, M S M E, Muhamad R F, et al. Design and Analysis of Jigs and Fixtures for Manufacturing Process[J]. IOP Conference Series: Materials Science and Engineering, 2019(551):12028.
[14] Avadhani S S, Rao S C, Kumara J C. Design of Special Fixture for Hard Chromium Plating on Internal Surface of Hollow Cylinder Open at One End and with Restricted Opening at the Other End with L/D Ratio More than 4[J]. Manufacturing Technology Today, 2019,18(S3):4-9.
[15] Edberk S A J, Shanmugam S N, Sankaranarayanasamy K. Design and fabrication of special fixture for different weld configurations of commercial pure Titanium sheet in laser beam welding process[J]. IOP Conference Series: Materials Science and Engineering, 2018,455(1):66-72.
[16] B L, G A, S A, et al. Cycle time reduction in manufacturing industry by designing a dedicated fixture: A case study[J]. International Journal of Engineering, Science and Technology, 2018,10(3):34.
[17] D. R K, T. B P, K. D B, et al. Design of a fixture for wire-cut EDM: A generic approach[J]. Materials Today: Proceedings, 2022,49(5):2034-2041.
[18] Jian S, Yu W, Houxiang H. CFETR Nb3Sn coil in heat treatment deformation analysis and fixture designing[J]. Journal of Physics: Conference Series, 2022,2181(1):33-37.
[19] Chandra B S C M, D. S K, S. D. Productivity improvement of a small scale industry by the application of an effective plant layout and weld-fixture design[J]. Materials Today: Proceedings, 2022,52(3):367-372.
[20] Luo J, Xiao Z T, Gong J W, et al. Special Fixture Designed for the Fine Boring of Auto Engine Cylinder[J]. Applied Mechanics and Materials, 2013,2659(395-396):990-995.

Publisher: Viser Technology Pte. Ltd.

URL: www.viserdata.com

Add.:111 North Bridge Rd, #21-01 Peninsula Plaza,

Singapore 179098

ISSN 2661-443X